Measurement of Surface Forces of Adsorbed Layers on Smooth Substrates

DISSERTATION

zur Erlangung des Grades eines Doktors der Naturwissenschaften

vorgelegt von

Dipl.-Phys. Volker Franz

aus Marl (Westfalen)

eingereicht beim Fachbereich Chemie – Biologie

der Universität Siegen

Siegen - 2001

1. Gutachter: Prof. Dr. H.-J. Butt

2. Gutachter: Prof. Dr. F. Schneider

3. Mitglied der Promotionskommission: Prof. Dr. H. J. Deiseroth

Datum der mündlichen Prüfung: 2. Februar 2002

1. Zusammenfassung

Mit dem Rasterkraftmikroskop (RKM) können Oberflächenkräfte experimentell einfach gemessen werden. Bei diesen Messungen nähern sich RKM-Spitze und Probe an, während die Kraft auf die Spitze aufgezeichnet wird. Die vorliegende Arbeit beleuchtet die dabei häufig beobachteten Einsprünge der Spitze des Rasterkraftmikroskops in Richtung des Substrats sowohl theoretisch als auch experimentell. Bekannt war, daß Einsprünge auftreten, wenn der Gradient einer attraktiven Oberflächenkraft die Federkonstante des RKM-Feder übersteigt. In dieser Arbeit wurde eine Nukleationstheorie entwickelt, die Einsprünge von RKM-Spitzen auf einem zweidimensionalen flüssigen Film auf einer Oberfläche beschreibt. Die Einsprünge entsprechen einem Durchbruch der Spitze durch den Film und sind thermisch aktiviert. Die Theorie sagt voraus, daß die Einsprungkraft mit steigender Annäherungsgeschwindigkeit der RKM-Spitze an das Substrat zunimmt. Parameter der Theorie sind die Anzahl der Durchstöße pro Sekunde der RKM-Spitze durch den flüssigen Film und ein aktiviertes Volumen. Experimentell werden zwei unterschiedliche Systeme untersucht. Ein thermisch aktivierter Einsprung wurde an Doppelschichten aus zwei Modell-Lipiden gefunden, die in Elektrolytlösung auf Glimmer adsorbiert sind. Für die Wechselwirkung zwischen RKM-Spitze und Glimmer beziehungsweise Graphit in *n*-Alkoholen mit zwei bis acht Kohlenstoffatomen wurde hingegen ein oszillierendes Kraftprofil nachgewiesen. Dieses Kraftprofil führt zu einem Einsprung, der nicht thermisch aktiviert ist. Aufgrund des Kraftprofils wurden Modelle für die Struktur der Alkoholmoleküle auf beiden Substraten entwickelt.

Abstract

The forces between surfaces determine the properties of many biological systems. This makes them an important field of study. With an atomic force microscope (AFM) such surface forces can be measured easily. In such measurements the AFM tip and the sample are approached and the force on the tip is recorded. It was the objective of this work to investigate the ubiquitous jumps of the tip towards the substrate both theoretically and experimentally. It is known that jumps occur if the gradient of an attractive force exceeds the spring constant of the cantilever. In this work a nucleation theory was developed that describes the jumps on a two-dimensional liquid film on a surface. These jumps correspond to the penetration of the tip through the liquid layer. The penetration is thermally activated. Theory predicts that the force at which the penetration occurs increases if the approach velocity between AFM tip and substrate increases. Parameters of the theory are the jump rate of the tip and an activated volume. Two different systems were investigated experimentally. A thermally activated jump was found for double layers of two model lipids, adsorbed on mica in electrolyte solution. Contrastingly, for the interaction between AFM tip and mica and graphite, both immersed in *n*-alcohols with 2 to 8 carbon atoms, a periodic force profile was found. This force leads to a jump that is not thermally activated. Models for the structure of the alcohol molecules on the substrates are proposed that are based on the force profile.

2. Introduction

All natural science is based on sensual perception and the desire to summarize as many observations as possible with few models. From the offspring of modern science researchers have tried to enlarge the areas that could be perceived. Since *Hans Lippershey's* invention of the telescope in 1608 it became possible to investigate the huge distances of the universe. Already some years earlier, about 1590, the Dutch glassmaker *Hans Janssen* disclosed the world on a small scale by his invention of the optical microscope. *Galileo Galilei* and *Antony van Leeuwenhoek* used the inventions in order to gain deeper insights of the world. Since then the possibilities to access natural phenomena by optical means evolved in an impressing way. For investigations on a small scale *Ernst Abbe* in 1866 could show theoretically that objects that are smaller than half a wavelength of the optical light were impossible to resolve further.

This discovery stimulated the research on other types of radiation that could be used to look at smaller structures. Especially since the discovery of the electron's wave properties the invention of the electron microscope by *Ernst Ruska* und *Max Knoll* led the pathway to modern electron microscopes that achieve images at atomic resolution. However, this resolution comes at the expense of a high vacuum that surrounds the sample. Especially for biological samples this limitation makes observations of living organisms impossible.

It was the invention of the atomic force microscope (AFM) by *Gerd Binnig, C. F. Quate,* and *Ch. Gerber* in 1986 (Binnig, Quate et al. 1986) that eliminated this limitation. Here, the surface of a sample is measured by scanning a small tip over it. This measurement technique allows not only to investigate the topology of a surface but also the forces that act between tip and surface. Thus, the AFM does not only allow to watch but also to *touch* specimens under investigation. A prominent example is the measurement of the mechanical strength of a single bond (Florin, Moy et al. 1994). Another application in biology is the use of the AFM in order to examine the adhesion of proteins on cell membranes (Müller, Butt et al. 2000).

Because of the difficulties to measure this interaction directly on the membranes of living cells the membranes are spanned onto solid substrates such as mica (Brian and McConnell 1984). These solid supported membranes can then be used as well reproducible model membranes. However, AFM experiments on lipid membranes are still lacking a complete understanding of the interaction of the tip with the bilayer. In all AFM measurements on lipid bilayers that came to my knowledge, e.g. (Dufrene, Boland et al. 1998; Müller, Butt et al. 2000; Schneider, Dufrene et al. 2000), it has been observed that the AFM tip approaches the surface of the lipid bilayer and then compresses it. If the force is continuously increased further finally a jump of the tip towards the substrate is observed (Figure 1). This jump has been interpreted as the break-through of the AFM tip through the bilayer until it comes to rest on the substrate. This hypothesis was supported by the observation that the jump height roughly corresponds to the thickness of a bilayer. However, the relation between the force at which the jump occurs and the physical properties of the bilayer was unknown because no quantitative model described the process. In this work, the jump of the tip through the bilayer is assumed to be possible if a hole forms under the tip that is big enough to allow for the break-through. The formation of a hole is kinetically hindered but thermal activation may eventually lead to the nucleation of a hole. Thus, a nucleation theory had to be developed.

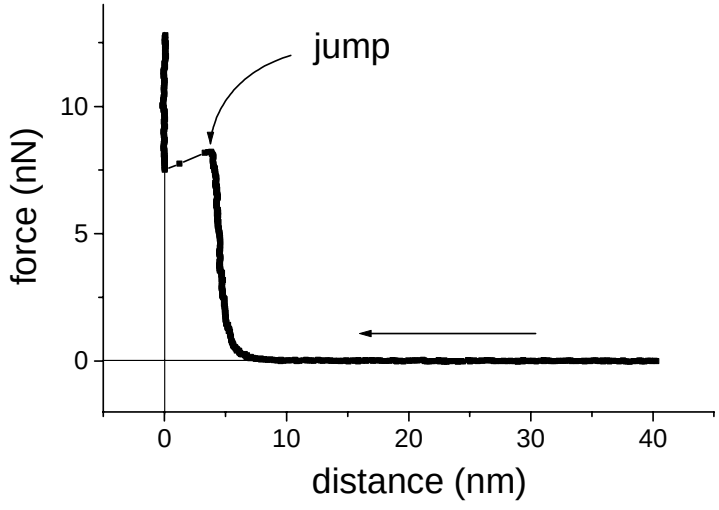

Figure 1. A typical measurement of the force between a AFM tip and a lipid bilayer. The tip approaches from large distances (arrow). At a certain distance the tip jumps discontinuously to the surface.

The possibility to 'touch' with the AFM, i.e. to measure forces, has made it possible to measure the forces over a substrate that are induced by the liquid structure. In such measurements often jumps have been reported, too. For example, for mixtures of *n*-alcohols with water a single jump can be observed as soon as the tip comes to a certain distance from the surface (Kanda 1998). Force measurements allow to test models for confined liquids in small gaps of 20 nm and below (Schoen 1998; Porcheron 2001).

It was the objective of this work to elucidate the mechanisms of the jump for the AFM tip. For the first time jumps have been described in the framework of a nucleation theory. It should be shown whether it is possible to distinguish between jumps that are simply due to large gradients of the forces on the tip and jumps that correspond to the penetration through a film. In this work two different systems were under study: Lipid bilayers on solid substrates immersed in electrolyte solution and pure *n*-alcohols on smooth substrates. The lipid bilayers were expected to represent liquid layers on a substrate while liquid *n*-alcohols are expected to have a structural order close to surfaces that prior to this work has not yet been measured.

The results of this work are not limited to the explanation of jumps that are observed in force measurements with an AFM. The nucleation theory that was developed can also be used as starting point for a microscopic theory of cutting. Generally, all results of this work contribute to a better understanding of confined liquid films.

In the **third chapter** the basic surface forces and the technical means to measure them, especially the AFM, are introduced. In the **fourth chapter** a nucleation theory for the penetration of an AFM tip through two-dimensional liquid films is developed. The distinction between jumps that are kinetically hindered and jumps due to mechanical instability is introduced. Then a nucleation theory for the jumps of the AFM tip is developed. Three different pressure distributions that the AFM tip exerts on the bilayer are inserted in the model. In the **fifth chapter** the theory is applied to force measurements on two types of lipid molecules. The **sixth chapter** is dedicated to the measurement of the forces between tip and smooth substrate, both being immersed in *n*-alcohols. The **seventh chapter** is a conclusion of the work.

3. Fundamentals

Surface Forces

In the following a brief introduction to surface forces shall be given.

Pauli repulsion

Due to the Pauli principle two electrons cannot occupy the same position in space. If they are brought in closer and closer proximity this repulsion is drastically increasing as soon as two particles of the two electronic orbitals would start to overlap. The Pauli repulsion is usually described by a hard-sphere potential or by an exponential law with a short decay length (smaller than 0.01 nm).

Electrostatic Forces

Between two charged bodies the electrostatic force is acting. In vacuum the force depends only on the geometry of the bodies. In aqueous electrolyte the Coulomb potential is screened by the ions in solution. The screening leads to an approximately exponential decay of the potential over a single charged surface in electrolyte solution. The exact equation for the electric potential at a distance x over a charged planar surface is the *Gouy-Chapman equation*

$$(1) \qquad \Psi(x) = \frac{2k_B T}{e} \log\left(\frac{1+\gamma\cdot\exp(-\kappa x)}{1-\gamma\cdot\exp(-\kappa x)}\right)$$

where $\kappa = \sqrt{\sum_{ions} \frac{\rho e^2 z_i}{\varepsilon\varepsilon_0 kT}}\ m^{-1}$ and $\gamma = \tanh\left(\frac{e\Psi_0}{4k_B T}\right)$.

The constants k_B, T, and e are Boltzmann's constant, temperature, and unit charge. ρ and z_i denote the number density in bulk of ions i in solution and the charge per ion. ε is the dielectric constant of the electrolyte and ε_0 is the permittivity of free space. Ψ_0 is the electric potential at the surface. For small surface potentials (Ψ_0 < 25 mV) the equation reduces to the *Debye-Hückel equation*

$$(2) \qquad \Psi(x) \approx \Psi_0 \cdot \exp(-\kappa x).$$

The decay length $1/\kappa$ of the potential is also known as *Debye length*. For a solution of a monovalent salt at a concentration of 1 mM at room temperature the Debye length is 9.6 nm. Increasing the concentration to 150 mM reduces the Debye length to only 0.8 nm.

Van der Waals Forces

Van der Waals forces between single molecules. The van der Waals force is a ubiquitous force between two arbitrary molecules. It consists of three contributions: The Keesom force between two permanent dipole moments, the Debye force between a permanent dipole and non-polar molecules, and the London dispersion force between two non-polar molecules. The latter force arises because the electronic charge distribution of any arbitrary molecule will fluctuate around the average coordinates. In general, this fluctuation leads to an asymmetric charge distribution. In turn, due to this asymmetry the molecule will acquire a dipole moment. The time-dependent dipole moment leads to a propagating electromagnetic wave that polarizes other molecules in its way. Eventually several dipoles are present that interact with each other. The dispersion force is the predominant of the three forces.

All three forces together make up the van der Waals force. An approximation for the non-retarded electromagnetic forces between two molecules embedded in a medium has been derived. The interaction energy at a distance r can be written as (Israelachvili 1992, p.96)

$$(3) \qquad w(r) = -\frac{C}{r^6}.$$

The factor C is a function of the material properties of the interacting molecules and the medium in which they are embedded.

For large distances between the interacting molecules the travel time for the electromagnetic wave may exceed the oscillation period of the dipole moment. In such a situation the electromagnetic wave, emanating from the first molecule and being reflected from the second molecule might find the first molecule with a dipole moment that does not lead to an attraction between them any more. Detailed analysis yields that such retardation effects lead to a dispersion force that decays like r^{-7}.

Van der Waals forces between a sphere and a surface. In force measurements the forces between single molecules are inaccessible. Instead the interactions between macroscopic bodies are measured. Here, the case of a sphere approaching a planar wall is considered.

In the theory first developed by Lifshitz the constant C in eq. (3) is expressed in terms of the *macroscopic* dielectric constants of tip, substrate and medium. The calculation has two steps: First, the interaction energy between one molecule of species *1* in the sphere and a wall consisting of many molecules of species *2* is computed. Secondly, the energy contributions of all molecules in the sphere are summed up. The result for the interaction energy W in dependence of the smallest distance between the surface of the sphere and the planar surface at small distances $D<R$ is (Israelachvili 1992, p.157)

$$(4) \qquad W(D) = -\frac{\pi^2 C \rho_1 \rho_2 R}{6D}.$$

The ρ_1 and ρ_2 denote the particle densities for the two media *1* and *2*. It is convenient to define the constant A as

$$(5) \qquad A = \pi^2 C \rho_1 \rho_2,$$

A is commonly called Hamaker constant. The van der Waals force $F = -\partial W/\partial D$ becomes

$$(6) \qquad F = -\frac{AR}{6D^2}.$$

Calculation of the Hamaker Constant. If the geometry is known, the main issue in the calculation of the van der Waals force is the evaluation of the Hamaker constant. In the framework of the Lifshitz theory the Hamaker constant can be expressed as an infinite series the first terms of which are

$$(7) \qquad A \approx \frac{3}{4} k_B T \left(\frac{\varepsilon_1 - \varepsilon_3}{\varepsilon_1 + \varepsilon_3}\right)\left(\frac{\varepsilon_2 - \varepsilon_3}{\varepsilon_2 + \varepsilon_3}\right) + \frac{3h}{4\pi} \int_{\nu_1}^{\infty} \left(\frac{\varepsilon_1(i\nu) - \varepsilon_3(i\nu)}{\varepsilon_1(i\nu) + \varepsilon_3(i\nu)}\right)\left(\frac{\varepsilon_2(i\nu) - \varepsilon_3(i\nu)}{\varepsilon_2(i\nu) + \varepsilon_3(i\nu)}\right) d\nu$$

Here, h is Planck's constant. The indices *1, 2, 3* denote the dielectric constants of sphere, substrate and the medium in between, respectively. The integration is carried out over all frequencies ranging from $\nu_1 = 2\pi k_B T/h$ to infinity.

The dielectric constant varies with frequency. For a dielectric medium it can be approximated by

$$(8) \qquad \varepsilon(i\nu) = 1 + \frac{n^2 - 1}{1 + \left(\frac{\nu}{\nu_e}\right)^2}.$$

Here, ν_e is the main electronic absorption frequency in the UV, that is typically around $3 \cdot 10^{15}$ s^{-1} and n is the refractive index of the medium.

For conducting media such as graphite an appropriate expression for the dielectric constant is

$$(9) \qquad \varepsilon(i\nu) = 1 + \left(\frac{\nu_p}{\nu}\right)^2.$$

Here, ν_p is the plasma frequency of the electrons.

A closed expression for the Hamaker constant can only be given in the case of three dielectric media or for two conductors interacting across vacuum. In general the integral (7) has to be solved numerically.

Van der Waals and electrostatic forces have been described together by Derjaguin, Landau, Verwey, and Overbeek. In the so-called DLVO theory (after the initials of its inventors) both forces are summed up.

Hertz theory

In 1881 *Heinrich Hertz* calculated pressures and displacements of a solid sphere with bulk elastic modulus E_1 that is pushed against a planar solid surface with a bulk elastic modulus E_2 (cf. Figure 2). No additional attractive or repulsive forces between the solids are considered. For the maximum pressure under the sphere the model predicts:

$$(10) \qquad \Delta p_{\max} = \frac{3}{2} \cdot \frac{F}{\pi a^2}.$$

Here, a is the radius of the circular contact region between sphere and plane, the so-called contact radius. It can be calculated to be

$$(11) \qquad a = \left(\frac{R \cdot F}{K^*}\right)^{\frac{1}{3}}.$$

R denotes the radius of the sphere and K^* is the joint elasticity modulus that is given by

$$(12) \qquad \frac{1}{K^*} = \frac{3}{4} \cdot \left(\frac{1-\upsilon_1^2}{E_1} + \frac{1-\upsilon_2^2}{E_2} \right),$$

where ν_i are the Poisson numbers of the materials. Pressure on the sphere leads to a indentation δ of the sphere. For geometrical reasons it is $\delta \approx a^2 / R$. Thus, the force on the tip in dependence of δ is given by

$$(13) \qquad F = R^{\frac{1}{2}} \cdot K^* \cdot \delta^{\frac{3}{2}}$$

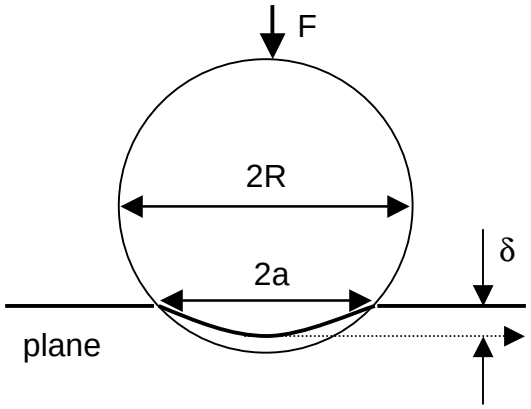

Figure 2. Geometry of a sphere with radius R that is pushed against a plane. Thereby it deforms the plane by δ. The contact radius is a.

Beyond Hertz theory

Based on Hertz' theory several other models have been developed. In the theory of Johnson, Kendall, and Roberts (JKR) the contact area is the same as in the Hertz theory but in the contact area adhesive forces act between sphere and substrate (Johnson, Kendall et al. 1971). Derjaguin, Muller, and Toporov (DMT) incorporate the pressure distribution of the Hertz model and assume additionally attractive van der Waals forces outside the contact area (Derjaguin, Muller et al. 1975). In both theories the frequently observed adhesion between particles is reproduced. The DMT theory suits better to soft materials while the JKR model is more appropriate if high elastic moduli are involved. Hertz theory describes contact forces suitably only if adhesive forces are negligible over elastic forces.

Johnson and Greenwood (Johnson and Greenwood 1997) expressed the conditions of validity of the individual theories more quantitatively. They state parameters that depend on the sphere radius, the elasticities, a characteristic atomic length scale, and the

work of adhesion. The parameters determine an appropriate model for the individual experimental situation.

The elastic foundation model

In general, the previous models are not valid for a rigid substrate with a thin soft layer on top. They can only be used as a first approximation if the deformations are small compared to the thickness of the soft layer. If this is not the case the soft layer with thickness *h* on a rigid substrate can be modelled by a series of elastic springs (Johnson 1985), p. 104. The situation is comparable to a soft mattress on a rigid floor (Figure 3). Neglecting any shear of the soft layer, Hooke's law takes the form

$$\Delta p = E \cdot \frac{\delta}{h}, \tag{14}$$

where h is the thickness and δ is the deformation of the layer. Assuming a spherical shape of the tip with a radius R at the apex of the tip, the deformation δ at a radial distance r from the tip apex is

$$\delta(r) = \delta_0 - \frac{r^2}{2R}. \tag{15}$$

Here, δ_0 denotes the maximum deformation under the tip. Now, the total force on the tip can be calculated according to

$$F = \int_S \Delta p \, dA = \int_0^a \frac{E}{h} \cdot \left(\delta_0 - \frac{r^2}{2R} \right) \cdot 2\pi r \, dr = \frac{2\pi E}{h} \left(\frac{\delta_0 a^2}{2} - \frac{a^4}{8R} \right). \tag{16}$$

S is the normal component of the interface between tip and layer while a denotes the contact radius of tip and layer and is given by

$$a = \left(2R\delta_0\right)^{\frac{1}{2}}. \tag{17}$$

Insertion of the expression for the contact radius into eq. (16) yields

$$F = \frac{\pi E R \delta_0^2}{h}. \tag{18}$$

Since $\Delta p_{\max} = E \cdot \frac{\delta_0}{h}$, eq. (18) leads directly to the dependence of the maximum pressure under the tip on the applied force:

$$\Delta p_{\max} = \left(\frac{EF}{\pi h R} \right)^{\frac{1}{2}}. \quad (19)$$

In this derivation sphere and substrate are assumed to be not deformable. Furthermore it is assumed that the soft layer only compresses in the normal direction and not horizontally. This means that the Poisson number ν of the soft layer is assumed to be zero.

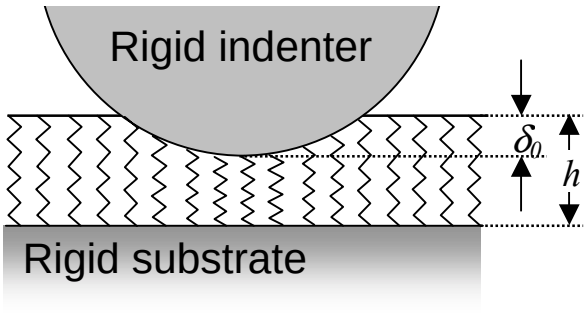

Figure 3. Illustration of the elastic foundation or 'mattress' model.

Elastic moduli in the Hertz semi sphere model and in the solid foundation model

In order to decide which model shall be used for a specific situation the dependence of the applied force on the deformation of the layer can be examined. Figure 4 shows the force that is necessary to deform the layer by a certain amount. The increase in the Hertz semi sphere model is less steep than the increase in the elastic foundation model but both models give similar concave graphs although both graphs have been calculated with different elastic moduli ($0.1 \cdot 10^9$ N/m^2 for the elastic foundation model, $0.7 \cdot 10^9$ N/m^2 for the Hertz semi sphere model). This shows that the elastic moduli depend strongly on the chosen model. Generally, for similar force versus compression curves, the Hertz semi sphere model provides higher values for the elastic modulus of the layer.

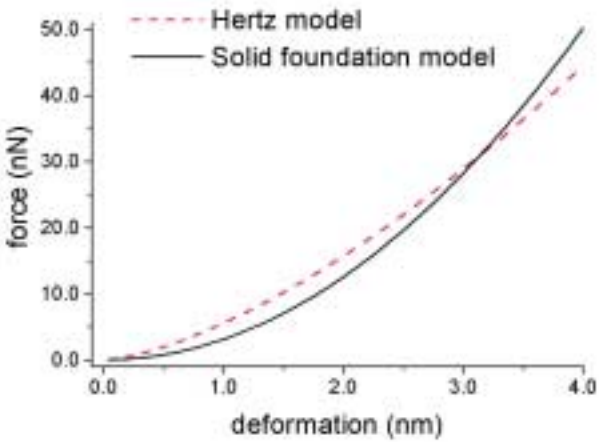

Figure 4. The force in dependence of the deformation. As elastic modulus $0.1 \cdot 10^9$ N/m^2 for the elastic foundation model (solid line), $0.7 \cdot 10^9$ N/m^2 for the Hertz semi sphere model (dashed line) are used. The radius is always R=40 nm. In the solid foundation model h=4 nm.

Solvation Forces

Solvation forces arise from the discrete molecular nature of the fluid molecules. They become important when a liquid is squeezed between two plates to a thickness D of less than a few nanometers. The DLVO theory breaks down in such small dimensions since the molecular structure of liquids cannot be neglected any more. The grand canonical potential Ω for this case is (Dijkstra 1998):

$$d\Omega = -p \cdot dV - S \cdot dT - N \cdot d\mu + 2 \cdot \gamma \cdot dA - f \cdot A \cdot dD \,. \tag{20}$$

The symbols have the following meaning: p is the pressure in the bulk liquid, dV is the differential of a volume, S is entropy, dT is the differential of temperature, N is the particle number, $d\mu$ the change in chemical potential, γ is the surface tension, dA the differential of the surface A, f denotes the solvation force, and dD the differential change of the height of the slit volume. Note that the solvation force has the unit of a pressure. From this equation follows

$$-\left.\frac{\partial \Omega}{\partial D}\right|_{V,T,A} = f \cdot A \,. \tag{21}$$

It was shown (Grimson and Richmond 1980) that for a single component fluid system the force depends only on the fluid density directly on the surfaces. The force results to be

$$f = \frac{k_B T}{2 \cdot \rho_0} \left(\rho^2(D) - \rho^2(\infty) \right). \tag{22}$$

The density function $\rho(D)$ denotes the density on the surface of one wall when the distance between the walls is D. ρ_0 is the bulk density of the liquid. This expression can describe an oscillating function. Generally, the density of a bath of particles oscillates in the vicinity of a solid wall which was demonstrated e.g. for spherical particles interacting by a Lennard-Jones potential (van Megen and Snook 1979) or hard rods (Grimson, Rickayzen et al. 1980). Under the assumption that the particle densities of two walls superimpose linearly in the slit, the density oscillations induced by the second wall will affect the density on the surface of the first wall and thus lead to oscillatory solvation forces.

The relation between the force f per unit area and the force F between a sphere with radius R and a plane at distance D is given by (Israelachvili 1992, p.162)

$$(23) \qquad F(D) \approx 2\pi R \cdot \int_{D}^{\infty} f(x)dx$$

Deriving both sides and rearranging yields

$$(24) \qquad f(D) = -\frac{1}{2\pi \cdot R} \cdot F'(H) .$$

Principally, the equation allows the determination of $\rho^2(D) - \rho^2(\infty)$ via eq. (22). Experimentally this equation is only of limited use because due to experimental noise it proves difficult to measure the force derivative $F'(D)$ with sufficient precision.

However, the work of adhesion *W(D)* is easily obtained by the Derjaguin approximation:

$$(25) \qquad F(D) \approx 2\pi R \cdot W(D) .$$

Scanning Force Microscopy

The main results in this work have been carried out with an AFM. The first AFM has been described in 1986 by Binnig, Quate, and Gerber (Binnig, Quate et al. 1986). It belongs to the still growing family of scanning probe microscopes, the first being the scanning tunneling microscope (Binnig, Rohrer et al. 1982).

Imaging

Figure 5 shows the basic set-up of an AFM. The surface under investigation is mounted on a piezoelectric translator. It is scanned line by line under a fine tip that usually has a tip radius 10-50 nm. The tip is mounted at the end of a microscopic cantilever (100-200 µm long, 0.5-1 µm thick) that has a triangular shape in the figure. Any force on the tip deflects the cantilever. The deflection can be measured by a laser beam that is reflected off the back side of the cantilever. The angle under which the laser beam is reflected depends on the deflection of the cantilever. Eventually, the laser beam impinges on a splitted photo diode. A deflection of the cantilever leads to a shift of the position of the reflected laser spot on the diode that can be detected by subtracting the voltages of the two parts of the diode. In the so-called 'contact mode' the z-piezo is regulated by a feed-back in a way that the signal of the splitted diode, i.e. the deflection of the cantilever, remains the same during a scan. The voltage at the z-piezo is recorded for every line scan and thus it delivers a set of height profiles. These profiles can be transformed into contour plots.

The AFM is a highly versatile instrument and this explains its widespread application. In particular it is easily possible to image structures in a liquid environment as required for biological applications. All measurements of this work have been carried out in liquid environment.

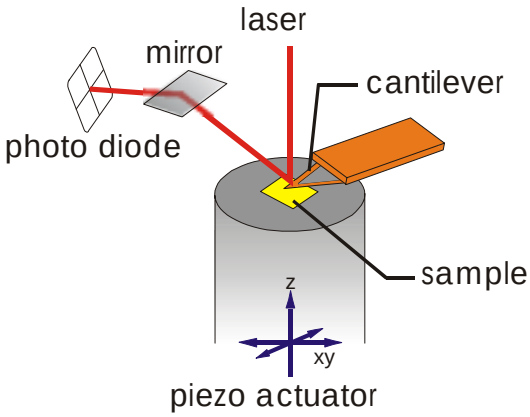

Figure 5. Sketch of an AFM set-up.

Image contrast and tip geometry

The AFM records deflections that a cantilever undergoes when the tip is scanned over a surface. Deflections can be due either to long range forces that may vary from one point to another of the surface of the sample or to topological protrusions. The force at which the cantilever is pressed against the surface can be chosen higher than all forces other than the Pauli repulsion if this does not influence the surface structure. This guarantees that the deflection is only caused by the topological structure.

The recorded deflection depends both on the structure of tip and surface. Figure 6a depicts the situation. The blunter the tip, the fewer details of the surface can be resolved. It is the tip radius that determines the maximum resolution of the image and this makes it important to know its size. The tip can be imaged in a transmission electron microscope (Butt, Döppenschmidt et al. 2000). Then the tip shape is fitted to a circle and its radius is measured. An alternative way to determine the tip shape is to image a surface structure that is sharper than the tip itself. In Figure 6b the situation shows is sketched. Spikes with small aperture angles are commercially available. The tip radius can be estimated by fitting several circles to sections of the tip profile as shown in Figure 7b. The tip radius is the radius of the smallest circle.

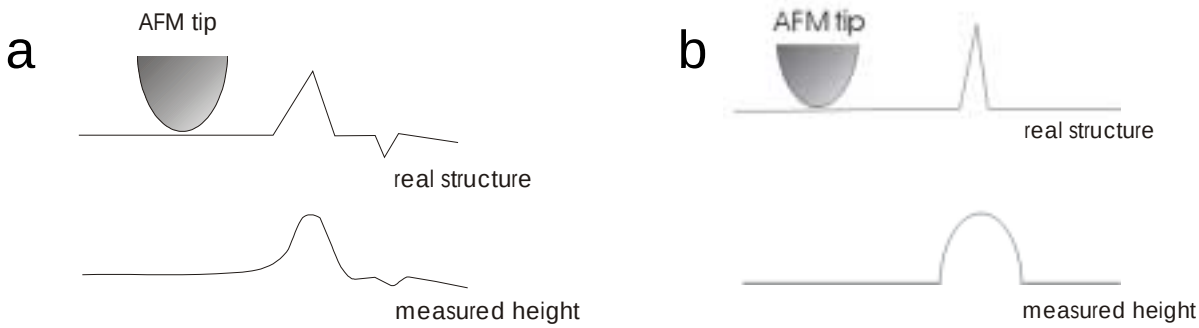

Figure 6. Imaging of a surface with an AFM tip. a) The image contains the shapes of surface and tip. The measured height does not exactly reproduce the real structure. b) The topology of the tip can be measured by imaging a spike with a small aperture angle.

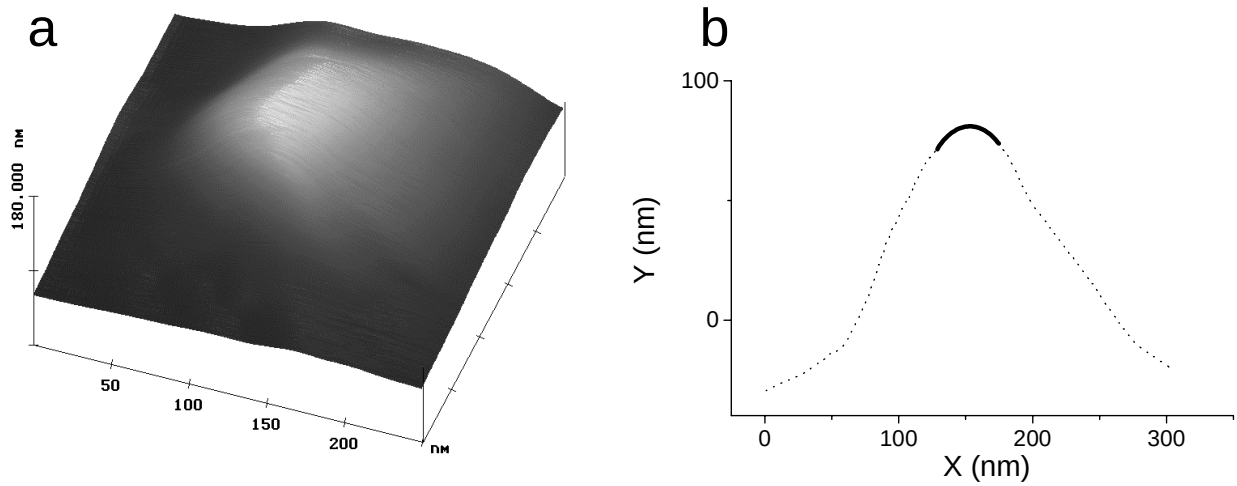

Figure 7. a) AFM image of a spike. The image corresponds to the surface of an AFM tip. b) Section through the image. A circular fit has been made through the apex of the section.

Force Measurements

In a force measurement, the sample is moved up and down by applying a voltage to the *z*-piezo. The cantilever deflection is recorded in volts. The voltage is arbitrary, depending on the exact position and shape of the reflex at the photodiode. The result of such a measurement is a deflection-piezo displacement plot which shows the cantilever deflection Δz_c vs. the position Δz_p of the piezo (Figure 8a). Such curves can be transformed into a plot like in Figure 8b that is a direct representation of the surface force between

tip and sample. Here, the force with which the cantilever is deflected is plotted versus the distance of the tip from the sample surface. The measured coordinates are transformed as follows. Here, an arrow ($\mapsto$) indicates a transformation step.

1. At very large distances the cantilever is not deflected and the data transform as follows:

$$\Delta z_c(\Delta z_p) \mapsto \Delta z_c(\Delta z_p) - \Delta z_c(\Delta z_{p\infty}) \tag{26}$$

$\Delta z_{p\infty}$ denotes a point where sample and tip are well separated.

2. The deflection is given as a voltage and it shall be transformed into a distance. For this purpose the fact is exploited that the deflection increases linearly with the position of the piezo translator as soon as the tip and the sample are in close contact. Thus, the slope m_{cc} of the straight line gives the factor that correlates the deflection in volts and the deflection in nanometers.

$$\Delta z_c(\Delta z_p) \mapsto \Delta z_c(\Delta z_p) / m_{cc} \tag{27}$$

3. The force shall be given in dependence on the distance d between tip apex and sample and not in dependence of the z-piezo position. From the geometry that is shown in Figure 9 it follows that

$$d - \Delta z_c + z_0 = \Delta z_p \,. \tag{28}$$

Thus, the z-coordinates must be transformed as

$$\Delta z_p \mapsto \Delta z_p + \Delta z_c - z_0 = d \tag{29}$$

4. The deflection is given in nanometers. In order to calculate the force that is applied to the cantilever the deflection has to be multiplied with the spring constant of the cantilever.

$$\Delta z_c(\Delta z_p) \mapsto \Delta z_c(\Delta z_p) \cdot K = F(\Delta z_p) \tag{30}$$

K denotes the spring constant of the cantilever.

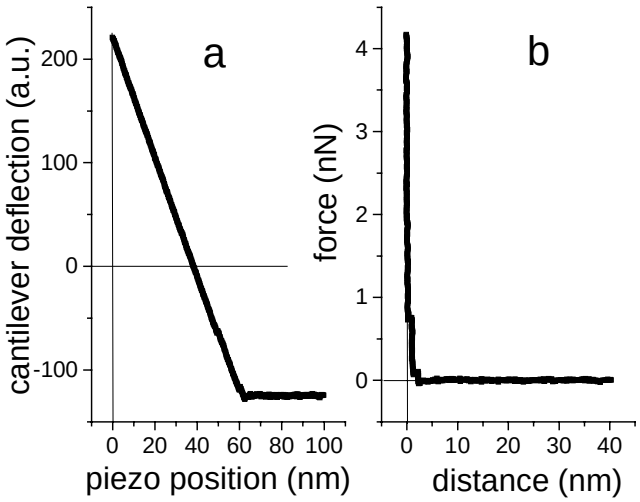

Figure 8. a) Deflection in arbitrary units versus the position of the z-piezo in nanometers. b) Calibrated force curve. Here, the force on the cantilever in nanonewton is plotted against the distance between tip and sample in nanometers.

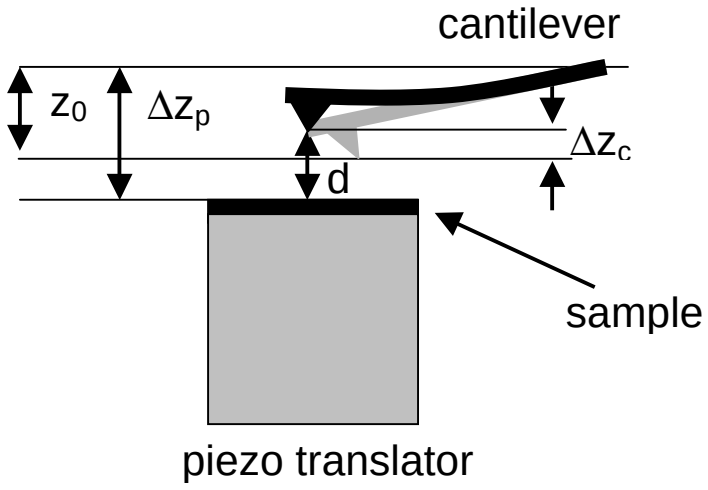

Figure 9. The geometry for the relation between piezo displacement Δz_p, cantilever deflection Δz_c out of its rest position, and distance d between tip of the deflected cantilever and sample is shown. z_0 is the arbitrary origin of the piezo displacement.

Measurement of the spring constant of the cantilever. Several methods for the determination of the spring constant have been described in the literature. The most straightforward method is the measurement of the Fourier spectrum of thermally excited oscillations, or *thermal noise*, of a cantilever. For cantilevers with a rectangular shape the spring constant can be calculated from the Fourier transform of the thermal noise (Butt 1995; Sader, Chon et al. 1999). The latter method allows the calculation of

the spring constant even without knowledge of the thickness of the cantilever that is not convenient to measure. However, the method can only be applied to cantilevers with a rectangular shape and not to triangular cantilevers that are used throughout this work. The spring constants of triangular cantilevers were calibrated according to another method (Torii, Sasaki et al. 1996). Here, the cantilever with the unknown spring constant and arbitrary shape is pushed against a rectangular reference cantilever, the spring constant of which has been measured from the spectrum of the thermal noise. Figure 10 shows the geometry of the calibration procedure that has two steps: The laser beam of the AFM is focussed on the back of the cantilever with the unknown spring constant. In a first step the cantilever is pushed against a solid substrate in order to obtain the proportionality factor m_{tc} between the displacement Δz of the piezo and the deflection: $\delta = m_{tc} \cdot \Delta z$. Then the cantilever under test is pushed against the reference cantilever and the signal

$$\delta_{test} = m_{tt} \cdot \Delta z_{tot} \qquad (31)$$

is recorded. Force equilibrium between the cantilevers requires that

$$\left(\delta_{tot} - \delta_{test}\right) \cdot k_{ref} = \cos\Theta \cdot \delta_{test} \cdot k_{test} . \qquad (32)$$

The absolute deflections δ_{test} and δ_{tot} are difficult to access. However, if tip and sample are in close contact not only eq. (31) but also

$$\delta_{tot} = m_{tc} \cdot \Delta z_{tot} \qquad (33)$$

is valid. Insertion of both equations in (32) yields

$$k_{test} = \frac{\left(m_{tc} - m_{tt}\right)}{\cos\Theta \cdot m_{tt}} \cdot k_{ref} . \qquad (34)$$

In the present work the spring constant k_{test} (throughout this work denoted K) of the cantilever has been measured individually for each cantilever. The error of the calibration of the cantilever spring constant has been estimated by making two measurements with different reference cantilevers and is about 20%. The error is mainly due to the fact that the tip of the cantilever touched the reference cantilever in different positions. The reference cantilever appears harder the more inwardly the cantilever touches it. This leads eventually to a higher spring constant of the cantilever under test.

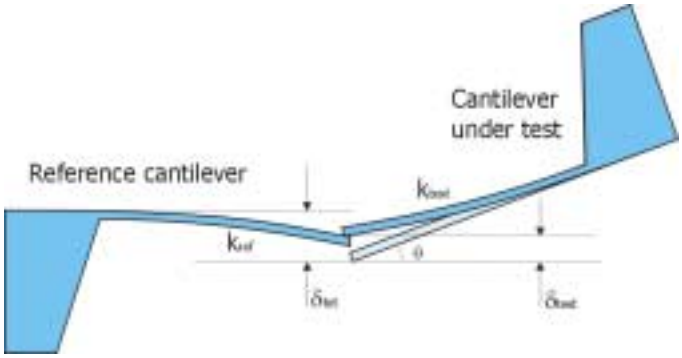

Figure 10. Sketch for the measurement of the spring constant. The cantilever under test is pushed against the reference cantilever with known spring constant.

Alternative Methods for Force Measurements

The AFM is not the only way to measure surface forces. Nowadays, several methods are commonly used (Claesson, Ederth et al. 1996). The AFM actually measures the forces between a sphere, i.e. the tip apex, and a flat surface. Its advantages are the possibility to image and to probe surface forces at the same time and its easy use.

In the *surface force apparatus* (SFA) (Tabor and Winterton 1968; Israelachvili and Tabor 1972) the forces between two cylinders with a radius of curvature of few centimeters are measured. The distance between the two mica sheets is measured by interferometry so that the substrate has to be transparent. Since the sheets come closely together over a considerable area the two surfaces have to be atomically smooth so that the distance is well-defined over the whole area. These practical reasons restrict the usable substrates to mica.

Laser tweezers offer the possibility to probe the interaction potential between two colloidal particles immersed in a solution (Grier 1997). The thermal oscillations of the colloidal particles depend on the potential between them. Therefore the measurement of these oscillations allow conclusions about the interparticle potential. However, presently the spatial resolution of these apparatuses is limited to some tens of nanometers.

Two-dimensional Liquid Layers on Surfaces

Molecules that adsorb from solution to a solid substrate can either move freely on the substrate or they are bound at a specific binding site. When they can move freely within the plane of the substrate they are classified as *two-dimensional liquids*. Typical examples are fluid lipid bilayers on smooth solid substrates such as mica. It depends on the

chain length, the saturation, and the head group if a lipid is fluid or solid. The higher the adhesion energy is, the higher the melting point becomes. Generally lipids with unsaturated oleoyl-groups are fluid at room temperature (Israelachvili 1992), p.378.

The movement of a molecule in a liquid consists of the following processes [Cohen, 1959 #263 ; Galla, 1979 #266)

1) A local free volume is created by density fluctuations that open up a hole in vicinity of a given molecule.
2) The given molecule jumps into this hole, creating a void at the previous position.
3) This lateral displacement is stabilzed by another molecule that fills the void.

The individual molecules change their place at the 'hopping rate' k. The hopping rate itself is governed by the activation energy that has to be overcome before a change of position can take place. The relation between hopping rate and activation energy is given by (Galla, Hartmann et al. 1979)

$$k = k_0' \cdot e^{-\frac{\Delta G}{k_B T}}. \qquad (35)$$

ΔG is the activation energy and k_0' a constant. The prefactor k_0' can be calculated from the sum of states in the framework of Eyring's theory of the activated complex and results to be $k_0' = \frac{k_B T}{h}$. Strictly speaking this is only valid if the reaction takes place in the gas phase. In liquids with strong interactions between the molecules the prefactor has to be modified (Wedler 1997), p. 922.

4. Mechanical Pressure on Lipid Bilayers: A Thermodynamic Approach

The objective of this work is to describe the frequently observed jumps in force curves that are measured on lipid bilayers. Figure 11 shows an exemplary curve that is taken on a bilayer that mimicks the membrane of cerebral cells (Müller, Butt et al. 2000).

Consider the AFM tip that approaches the lipid bilayer. Before the tip approaches the bilayer both tip and layer are well separated and no force is acting between them. The cantilever is not deflected at all. The bilayer in this state has a Gibbs energy G_i. Decreasing the distance between layer and tip further eventually leads to contact between them and to an increase of the pressure that the tip exerts on the bilayer. The Gibbs energy of the bilayer with the tip in contact is still G_i neglecting any elastic deformation of the bilayer. Now the pressure Δp is exerted upon the bilayer and the initial energy level is increased by $V\Delta p$. At a certain level it exceeds the Gibbs energy of the bilayer after penetration of a tip, G_f. Once G_i being bigger than G_f, a break-through can occur. The change in elastic energy of the cantilever during the break-through can be neglected because it remains almost constant.

Now, two fundamentally different cases can occur. In a first scenario the molecules in the bilayer simply follow the potential gradient and move to an energetically more favourable position. Thereby they open a hole into which the tip can jump.

As alternative scenario the new energetical minimum of the molecules might be kinetically hindered because an energy barrier has to be overcome. Both cases will be examined in the following.

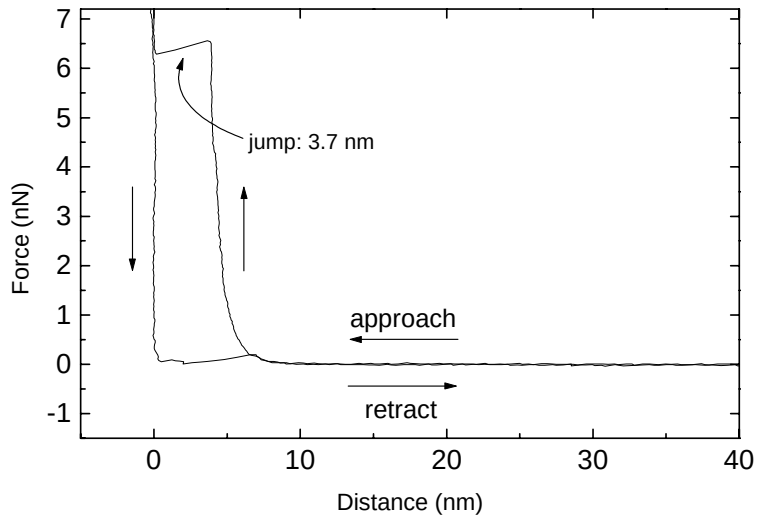

Figure 11. Typical force curve on a lipid bilayer, reproduced from (Müller, Butt et al. 2000).

No kinetic barrier: The direct passage

If there is no activation barrier for the molecules that change their places or if the activation barrier is smaller than $k_B T$ at room temperature, then the molecules move fast once it has become thermodynamically favourable for them ($G_f < G_i$). Under the assumption of no energy barrier jump-ins can be well explained as mechanical instabilities that occur whenever small oscillations of the cantilever around its actual position are not damped out but amplified. To the best of my knowledge this case has been assumed for all jump-ins that have been reported previously in literature, cf. (Gady, Schleef et al. 1998; Cappella and Dietler 1999).

In Figure 12 an arbitrary surface force profile is drawn. In two points of the curve the force is plotted that has to be exerted in order to move the cantilever by a certain distance (dotted lines). The slope corresponds to the spring constant of the cantilever. The difference between the force profile and the force that is needed to deflect the cantilever is the force that accelerates the tip (solid lines). Consider an approach of a probe from large distances, i.e. the tip moves on the curve from the right to the left. Point 1: A small shift downwards leads to a repulsive resulting force while an upward shift leads to an attractive resulting force. Thus, in this point the tip is stable. In point 2 the situation is quite different: A downward shift leads to a negative resulting force that drives

the tip further down. In this situation the tip jumps. The jump is slowed down as soon as the resulting force becomes positive again.

Thus, purely mechanical considerations lead to a jump-in of the tip. Generally, jumps occur when in a point on the force profile the force becomes more attractive than the force that is needed to deflect the cantilever. In the absence of an activation barrier for the movement of the molecules, the break-through force depends solely on the shape of the surface potential and not on any other experimental parameter, e.g. the approach speed.

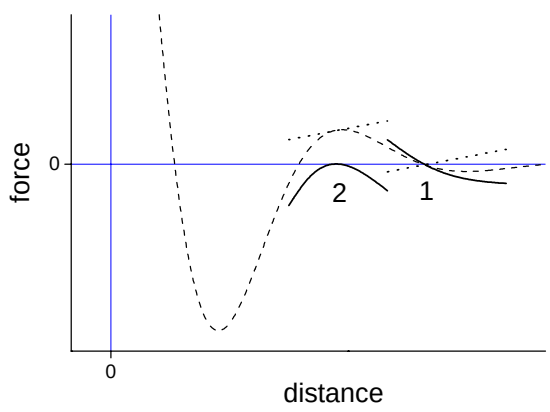

Figure 12. Arbitrary surface force profile for an AFM tip (dashed line). On two points the force is plotted that has to be applied in order to shift the tip by a certain distance (dotted lines). The solid lines represent the resulting forces on the tip. Point 1: Stable position. Point 2: Metastable position.

Occurrence of a kinetic barrier

If the process is kinetically hindered, an activation energy that is bigger than the thermal energy $k_B T$ has to be overcome before a sufficient number of molecules can move at the same time to a thermodynamically favourable position. The kinetic barrier is the fingerprint of a transition state through which the molecules have to go before a hole can be formed. For the penetration of an AFM tip through a lipid bilayer on a substrate the the creation of a hole in the bilayer costs energy. On the other hand, energy will be gained when the lipid molecules move out of the area of high pressure under the tip. Thus the energetically unfavourable transition is the formation of a hole in the lipid bilayer.

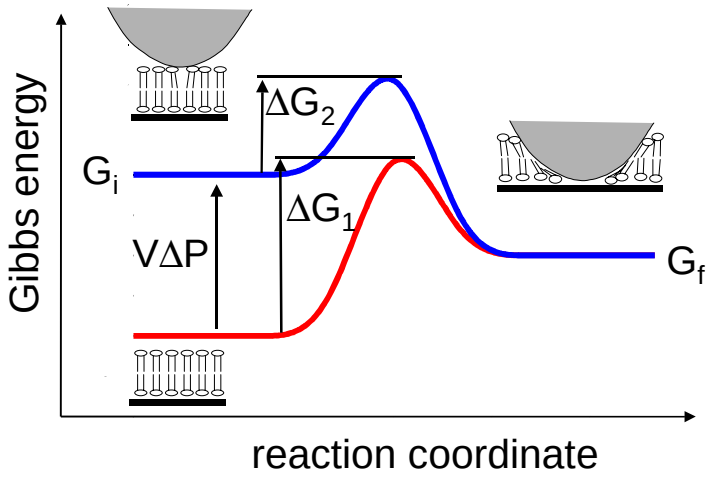

Figure 13. The change of Gibbs energy during the break-through of the tip through the bilayer. The lower curve denotes the energy change for placing a tip into the bilayer. Initially it is thermodynamically unfavorable because the final energy is higher than the initial energy. If pressure is exerted on the bilayer the energy follows the upper curve. The liquid under the tip experience an increase in Gibbs energy by $V\Delta p$ and the energy barrier is lowered from ΔG_1 to ΔG_2.

The velocity of the break-through can be increased if the activation barrier is lowered. This is a collateral effect of increasing the energy level of the initial state with respect to the final energy level. An energy shift by ΔG leads to a reduction of the activation energy by $\alpha\Delta G$ ($0<\alpha<1$) from ΔG_1 to ΔG_2. The construction is shown in Figure 14.

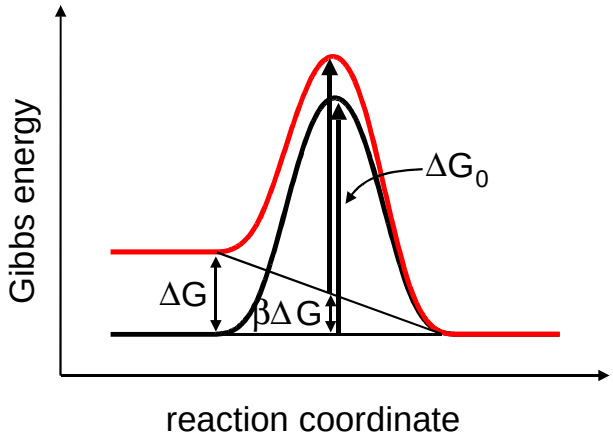

Figure 14. Lowering of the activation barrier: The initial energy is raised by ΔG. The new activation barrier has the height $\Delta G_0+\beta\Delta G-\Delta G$. This means that the activation barrier has been lowered by $(1-\beta)\Delta G=\alpha\Delta G$. For a symmetric barrier $\alpha=0.5$.

In the following an expression for the probability of the break-through in dependence of the applied pressure on the lipid bilayer is derived. Therefore, I consider an ensemble of N_0 identical systems. Each system consists of AFM tips on a lipid bilayer. Every tip exerts a growing force on the bilayer. After a time t has elapsed, N bilayers remain that did not undergo a break-through. t=0 denotes the time when the tip gets into contact with the bilayer but the pressure is still zero. Within the time interval dt this number is reduced by dN since $|dN|$ tips penetrate through the bilayer. $|dN|$ is proportional to the number N of intact bilayers, the rate constant k, and the time interval dt:

$$(36) \qquad dN = -k \cdot N \cdot dt$$

In general, k is time-dependent. Dividing by N_0 one changes to probabilities:

$$(37) \qquad dP = -k(t) \cdot P \cdot dt\,,$$

where $P=N/N_0$ is the probability to find a tip on top of the bilayer. At $t=0$ we have P=1. This differential equation can be integrated to give

$$(38) \qquad \ln P(t) = -\int_{t_0}^{t} k(t')dt'\,.$$

For the sake of generality the integration is performed from t_0 to t. At the time t_0 the break-through becomes energetically possible, i.e. $G_f < G_i$. The rate constant k follows the Arrhenius law

$$(39) \qquad k(t) = k_0' \cdot e^{-\frac{G^*}{k_B T}} = k_0' \cdot e^{-\frac{G_0^* - \Delta G(t)}{k_B T}} \equiv k_0 \cdot e^{\frac{\Delta G(t)}{k_B T}}\,.$$

Here, G^* is the Gibbs' activation energy necessary for the nucleation of a hole in the bilayer. k_0' is the above-mentioned constant that is introduced in the framework of Eyring's theory of the activated complex and k_0 is the hole formation rate when no pressure is applied. Consider that G^* is reduced by $\Delta G(t)$ from its unperturbed value $G_0{}^*$. For the case of a tip pressing on a bilayer $\Delta G(t)$ is given by

$$(40) \qquad \Delta G(t) = \alpha \cdot \Delta p(t) \cdot V$$

The factor α is a geometrical factor that expresses the fact that not the whole work of pressure lowers the activation barrier but only a fraction of it. This fraction depends on the shape of the activation barrier and is 0.5 for a symmetrical barrier. V is the activated volume. Inserting eqs. (39) and (40) in (38) leads to

$$\ln P(t) = -\int_{t_0}^{t} k_0 \cdot e^{\frac{\alpha \cdot \Delta p(t) \cdot V}{k_B T}} dt' \qquad (41)$$

In order to calculate the probability explicitly, the time dependence of the maximum pressure under the tip, *Δp(t)*, has to be known. For this purpose three models are presented and discussed (Figure 15): The first is the *stamp model* in which we model the tip as a flat plane that is in close contact with the bilayer. The second is the *Hertz semi-sphere model* in which the more realistic assumption is made that the tip is a semi-sphere that pushes on the lipid bilayer. However, the bilayer and substrate are treated as being of the same material. The third model is the *elastic foundation* model that models the bilayer as an ensemble of elastic springs onto which a sphere is exerting pressure.

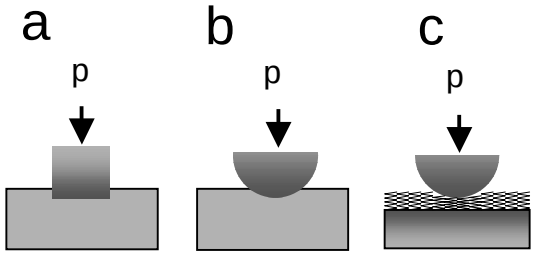

Figure 15. Illustration of the three models: a) Flat stamp model. b) Hertz semi sphere model. c) Solid foundation model.

A nucleation theory with the flat stamp model

In this approximation a uniform pressure distribution in the contact region is assumed. Thus $\Delta p = F(t)/A$, where A is the area over which the pressure is exerted. Once the tip is in contact with the lipid bilayer, the force of the tip on the bilayer is $F(t) = K \cdot \Delta z_c$, where K is the spring constant of the cantilever and Δz_c is its deflection. As the sample moves at constant velocity v referring to the base of the cantilever, the deflection of the cantilever is $\Delta z_c = v \cdot t$. Thus, the time dependence of the pressure during the approach is

$$\Delta p = \frac{k \cdot v \cdot t}{A}. \qquad (42)$$

Combining equations (41) and (42) leads to

$$(43) \qquad \ln P(t) = -k_0 \cdot \frac{A \cdot k_B T}{\alpha V \cdot Kv} \cdot \left[\exp\left(\frac{\alpha V}{k_B T} \cdot \frac{Kv \cdot t}{A} \right) - \exp\left(\frac{\alpha V}{k_B T} \cdot \frac{Kv \cdot t_0}{A} \right) \right].$$

Since the break-through is usually represented in terms of force rather than in terms of time, t is substituted by $t = F/Kv$:

$$(44) \qquad P(F) = \exp\left[-k_0 \cdot \frac{A}{\alpha V} \cdot \frac{k_B T}{Kv} \left(\exp\left(\frac{1}{k_B T} \cdot \frac{\alpha V}{A} \cdot F \right) - \exp\left(\frac{1}{k_B T} \cdot \frac{\alpha V}{A} \cdot F_0 \right) \right) \right].$$

Here, F_0 is the force at time t_0 from which on a jump to the surface becomes energetically possible. $P(F)$ denotes the total probability that the tip did not penetrate the bilayer at a given force F when a cantilever is moved at constant approach velocity v towards the sample. It is convenient to introduce the abbreviation

$$(45) \qquad F_T = \frac{A}{\alpha V} \cdot k_B T .$$

One obtains

$$(46) \qquad P(F) = \exp\left[-F_T \cdot \frac{k_0}{Kv} \left(\exp\left(\frac{F}{F_T} \right) - \exp\left(\frac{F_0}{F_T} \right) \right) \right]$$

From this equation several experimentally accessible parameters can be obtained.

Average probability

The average break-through force F_{av} is given by

$$(47) \qquad F_{av} = \int_0^\infty P_{jump}(F) \cdot F \, dF .$$

The probability P_{jump} for a break-through to occur at force F is given by the negative derivative of the total probability

$$(48) \qquad P_{jump} = -\frac{\partial P}{\partial F} .$$

Hence,

$$(49) \qquad P_{jump} = \frac{k_0}{Kv} \cdot \exp\left[\frac{F_T \cdot k_0}{Kv} \left(\exp\left(\frac{F_0}{F_T} \right) - \exp\left(\frac{F}{F_T} \right) \right) + \frac{F}{F_T} \right]$$

Equation (47) cannot be integrated analytically. Therefore the additional approximation is made that the jump occurs when $P(F_{av})$=0.5. Inserting this condition in eq. (49) gives

$$(50) \qquad F_{av} \approx F_T \cdot \ln\left[\frac{\ln 2 \cdot K}{k_0 \cdot F_T} \cdot v + \exp\left(\frac{F_0}{F_T}\right)\right].$$

Width of probability distribution

The half-width of the probability distribution is given by the forces F that satisfy the condition

$$(51) \qquad P_{jump}(F) = \frac{P_{jump}(F_{av})}{2}.$$

This equation can only be evaluated numerically. It is found that the width depends on k_0 and $A/\alpha V$ but it is independent on the velocity of the tip.

Evaluation of k_0 and $A/\alpha V$

The dependence of F_{av} on the approaching velocity that is predicted by eq. (50) can be further simplified. Two extreme cases can be considered. The first is that $\frac{\ln 2 \cdot K}{k_0 \cdot F_T} \cdot v$ can be neglected over $\exp\left(\frac{F_0}{F_T}\right)$. Then

$$(52) \qquad F_{av} = F_0.$$

Hence, the average break-through force is a constant and equal to the threshold force F_0. Note that this approximation is valid when k_0 becomes very large, i.e. when the activation barrier disappears. Hence, the nucleation theory contains also the case of the direct passage when no kinetic barrier is present and jumps are exclusively caused by an attractive surface potential.

In the opposite extreme we can set F_0=0 and neglect $\exp\left(\frac{F_0}{F_T}\right)$ over $\frac{\ln 2 \cdot K}{k_0 \cdot F_T} \cdot v$. In this case one obtains

$$(53) \qquad F_{av} = F_T \cdot \ln\left[\frac{\ln 2 \cdot K}{k_0 \cdot F_T} \cdot v\right].$$

Here, F_{av} depends logarithmically on the velocity v. The parameters k_0 and $A/\alpha V$ can be calculated from a fit to

$$(54) \qquad F_0 = a + b \cdot \log v \,.$$

Comparison of equations (53) and (54) leads to

$$(55) \qquad \frac{A}{\alpha V} = \frac{\log e \cdot b}{k_B T} \text{ and}$$

$$(56) \qquad k_0 = \frac{\ln 2 \cdot K}{\log e \cdot b} \cdot 10^{-\frac{a}{b}} \cdot \frac{m}{s} \,.$$

After determining a and b from the experimental results $A/\alpha V$ and k_0 can be calculated.

Illustration of the results

Apart of the values of the values of the parameters it turns out that the results for the flat stamp model are qualitatively similar to those for the other models that are derived below. Differently from the other models the functions P, P_{jump} and F_{av} can be calculated *analytically* for the flat stamp model. This has been done for a set of arbitrarily chosen parameters ($A/\alpha V$=0.5·10^{11} m^{-1}, k_0=10^{-5} s^{-1}, K=0.1 N/m, v=1 µm/s). The result for P and P_{jump} is shown in Figure 16 and Figure 17. Two threshold forces, F_0=0 nN and F_0=3.5 nN, have been assumed.

The probability density for a jump is a bell-shaped curve. If the threshold force is larger than zero the function P_{jump} is zero up to the threshold force where it is discontinuous. Note that the integral of P_{jump} is 1 since it is a probability density.

The average break-through force increases with increasing approach velocity. The graph for F_0=0 nN reflects the fact that for low velocities the break-through force is given by the threshold force.

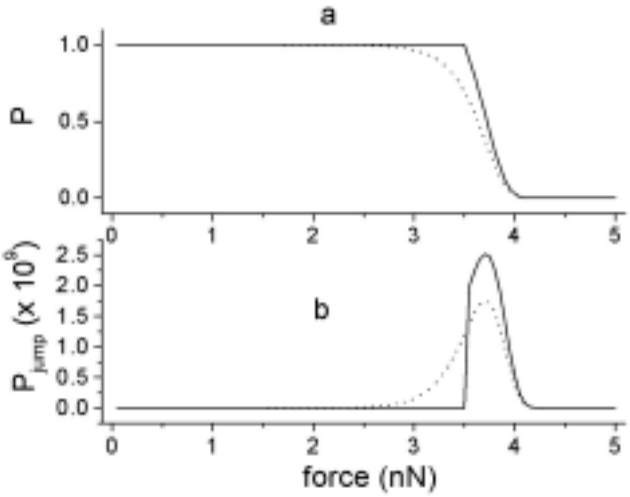

Figure 16. a) Probability P that tip rests on top of the bilayer at a given force. Dotted curve: F_0=0 nN. Solid curve: F_0=3.5 nN. b) Probability density P_{jump} that the tip jumps at a given force. Dotted curve: F_0=0 nN. Solid curve: F_0=3.5 nN.

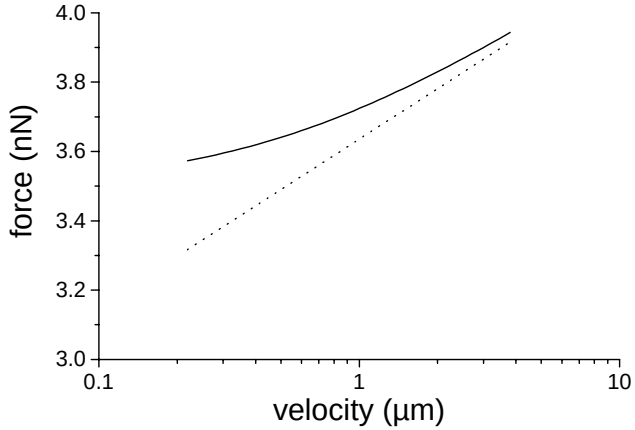

Figure 17. Dependence of the break-through force in dependence on the approach velocity. Dotted line: F_0=0 nN. Solid line: F_0=3.5 nN.

The retract

The probability for the jump out of the tip can be computed in an analogous manner. Note that a jump-out is contrary to the adhesion of the tip to the substrate. It occurs if the hole in the bilayer closes spontaneously although the tip is still pressing against the substrate.

Again, the starting point is the integral in eq. (41). During the retract the pressure decreases in time as

$$\Delta p(t) = \frac{F_0^r - K \cdot v \cdot t}{A}. \qquad (57)$$

F_0^r is the threshold force from which a jump-back is considered possible. Evaluating the integral eventually leads to

$$(58) \qquad \ln P(F) = \frac{k_0^r \cdot F_T^r}{K \cdot v} \cdot e^{\frac{F_0}{F_T^r}} \cdot \left(e^{\frac{F - F_T^r}{F_T^r}} - 1 \right).$$

Again, this expression can be used to calculate the average break-through force. The integral (47) cannot be given analytically but making use of the above approximation $P(F_{av})$=0.5 yields

$$(59) \qquad F_{av}^r = F_0^r + F_T^r \cdot \ln\left(1 - v \cdot \frac{\ln 2 \cdot K \cdot e^{-\frac{F_0}{F_T^r}}}{k_0^r \cdot F_T^r} \right).$$

Figure 18 shows the function $F_{av}^r = F_0^r + 1 \cdot \ln(1 - 1 \cdot x)$. From the graph it can be seen that F_{av}^r is a monotonously decreasing function of v. The limit of the average detachment force for the velocity approaching zero is the threshold force F_0^r that thus can be experimentally accessed by measuring the detachment force for very small velocities.

In general, the threshold forces F_0 and F_0^r for the approaching part and for the retracting part are not the same. The same holds for the parameters k_0^r and F_T^r that are not equal to the corresponding parameters during the approach.

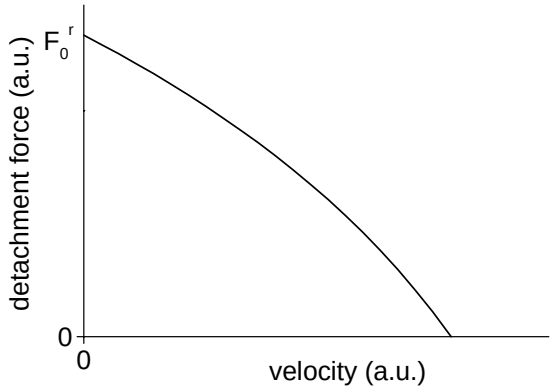

Figure 18. The function $F_{av}^r = F_0^r + 1 \cdot \ln(1 - 1 \cdot x)$ that describes the retract part of the force curves if a threshold force F_0^r exists.

A nucleation theory with the elastic foundation model

The bilayer is modelled as a layer of springs on a hard substrate. The elastic modulus of the tip is also infinitely hard. Presumably the break-through occurs at the point under the tip with the highest pressure. The maximum pressure is calculated by inserting eq. (17) into eq. (19):

$$(60) \qquad \Delta p_{\max} = \left(\frac{EF}{\pi h R} \right)^{\frac{1}{2}}.$$

Inserting this in eq. (41) gives

$$(61) \qquad \ln P(t) = -\int_{t_0}^{t} k_0 \cdot e^{\frac{\alpha \cdot V}{k_B T} \cdot \left(\frac{E}{\pi h R} \right)^{\frac{1}{2}} \cdot F^{\frac{1}{2}}} dt'.$$

It is convenient to define a 'thermodynamic force'

$$(62) \qquad F_T^S = \frac{\pi \cdot h \cdot R}{E} \cdot \left(\frac{k_B T}{\alpha V} \right)^2$$

so that the integral becomes

$$(63) \qquad \ln P(F) = -\frac{k_0}{Kv} \cdot \int_{F_0}^{F} e^{\left(\frac{F'}{F_T^S} \right)^{\frac{1}{2}}} dF'.$$

This integral can be solved analytically by substitution and partial integration to obtain

$$(64) \qquad \ln P(F) = -\frac{2 k_0 F_T^S}{Kv} \cdot \left[e^{\left(\frac{F}{F_T^S} \right)^{\frac{1}{2}}} \cdot \left(\left(\frac{F}{F_T^S} \right)^{\frac{1}{2}} - 1 \right) - e^{\left(\frac{F_0}{F_T^S} \right)^{\frac{1}{2}}} \cdot \left(\left(\frac{F_0}{F_T^S} \right)^{\frac{1}{2}} - 1 \right) \right].$$

For the probability of a break-through at a force F one obtains according to eq. (48)

$$(65) \qquad P_{jump}(F) =$$

$$\frac{k_0}{Kv} \cdot \left(1 + \left(\frac{F_T^S}{F} \right)^{\frac{1}{2}} \right) \cdot \exp\left[-\frac{2 k_0 F_T^S}{Kv} \left(e^{\left(\frac{F}{F_T^S} \right)^{\frac{1}{2}}} \cdot \left(\left(\frac{F}{F_T^S} \right)^{\frac{1}{2}} - 1 \right) - e^{\left(\frac{F_0}{F_T^S} \right)^{\frac{1}{2}}} \cdot \left(\left(\frac{F_0}{F_T^S} \right)^{\frac{1}{2}} - 1 \right) \right) + \left(\frac{F}{F_T^S} \right)^{\frac{1}{2}} \right]$$

As for the flat stamp model and for the Hertz semi sphere model the calculation of αV and k_0 from the average break-through forces is analytically impossible. Therefore the approximation $P(F_{av})=0.5$ shall be used. One obtains

$$(66) \qquad \ln 0.5 = -\frac{2 k_0 F_T^S}{Kv} \cdot \left[e^{\left(\frac{F_{av}}{F_T^S} \right)^{\frac{1}{2}}} \cdot \left(\left(\frac{F_{av}}{F_T^S} \right)^{\frac{1}{2}} - 1 \right) - e^{\left(\frac{F_0}{F_T^S} \right)^{\frac{1}{2}}} \cdot \left(\left(\frac{F_0}{F_T^S} \right)^{\frac{1}{2}} - 1 \right) \right].$$

This equation contains the three unknown parameters k_0, F_T, and F_0. F_T is related to αV. Equation (66) cannot be solved analytically. Hence, the unknown k_0, αV and F_0 can only be extracted numerically. Eq. (66) can be rearranged to give

$$(67) \qquad k_0 = \frac{\ln 2 \cdot Kv}{2 \cdot F_T^S \cdot \left[e^{\left(\frac{F_{av}}{F_T^S}\right)^{\frac{1}{2}}} \cdot \left(\left(\frac{F_{av}}{F_T^S}\right)^{\frac{1}{2}} - 1 \right) - e^{\left(\frac{F_0}{F_T^S}\right)^{\frac{1}{2}}} \cdot \left(\left(\frac{F_0}{F_T^S}\right)^{\frac{1}{2}} - 1 \right) \right]}.$$

For simplicity it is assumed that F_0=0 N. This assumption will be justified *a posteriori* by the measurements. If F_0=0 N then two equations can be generated from eq. (67) by inserting two measured values for the velocity v and the break-through force F_{av}. By equating the two equations the parameter k_0 is eliminated. Then the new equation can be solved numerically or graphically for F_T^H. From F_T^H the activated volume αV can be calculated. Inserting F_T^H and one pair (v, F_{av}) from the measurements into eq. (67) eventually gives k_0.

The retract

The force for detaching the cantilever from the surface can be calculated analogously to the break-through force during the approach. However, the physical situation is much better described in the flat stamp nucleation model than in the solid foundation nucleation model. Unlike during the approach the contact area does not change considerably while the cantilever is pulled away from the surface. Since the cantilever adheres tightly on the surface the contact area is expected to change only immediately prior to the jump-out. Thus, the stamp model that assumes a constant contact area during the detachment process fits the physical situation well.

A nucleation theory with the Hertz semi sphere model

Here the pressure of a sphere on a layer is modelled for the case that both sphere and bilayer consist of different, but homogeneous materials. The sphere is infinitely hard. Assume that the break-through will start at the point under the tip where the pressure is maximal. Insertion of eq. (11) into (10) gives

$$(68) \qquad \Delta p_{\max} = \frac{3}{2} \cdot \frac{F^{\frac{1}{3}} \cdot K^{*\frac{2}{3}}}{\pi R^{\frac{2}{3}}} \equiv C \cdot F^{\frac{1}{3}}.$$

For simplicity the constant $C = \dfrac{3 \cdot K^{*\frac{2}{3}}}{2\pi \cdot R^{\frac{2}{3}}}$ is introduced. Insertion of this result into eq. (41) yields

$$\ln P(t) = -\int_{t_0}^{t} k_0 \cdot e^{\frac{\alpha \cdot V \cdot C \cdot F(t')^{\frac{1}{3}}}{k_B T}} dt' . \tag{69}$$

The force increases as $F=K \cdot v \cdot t$ so that the time variable can be substituted. Hence

$$\ln P(F) = -\frac{k_0}{K \cdot v} \int_{F_0}^{F} e^{\frac{\alpha \cdot V \cdot C \cdot F'^{\frac{1}{3}}}{k_B T}} dF' . \tag{70}$$

Finally, it is convenient to introduce a new parameter, the thermodynamic force F_T^H. It is defined by

$$F_T^H = \left(\frac{k_B T}{\alpha \cdot V \cdot C} \right)^3 = \frac{8\pi^3 \cdot (k_B T)^3 \cdot R^2}{27 \cdot \alpha^3 \cdot V^3 \cdot K^{*2}} . \tag{71}$$

With this definition one obtains

$$\ln P(F) = -\frac{k_0}{K \cdot v} \int_{F_0}^{F} e^{\left(\frac{F'}{F_T^H} \right)^{\frac{1}{3}}} dF' . \tag{72}$$

The integral can be solved analytically by substitution and subsequent partial integration. The result is

$$\begin{aligned} \ln P(F) = \frac{3 \cdot k_0}{K \cdot v} F_T^H \cdot \Bigg[& e^{\left(\frac{F_0}{F_T^H} \right)^{\frac{1}{3}}} \cdot \left(\left(\frac{F_0}{F_T^H} \right)^{\frac{2}{3}} - 2 \cdot \left(\frac{F_0}{F_T^H} \right)^{\frac{1}{3}} + 2 \right) \\ & - e^{\left(\frac{F}{F_T^H} \right)^{\frac{1}{3}}} \cdot \left(\left(\frac{F}{F_T^H} \right)^{\frac{2}{3}} - 2 \cdot \left(\frac{F}{F_T^H} \right)^{\frac{1}{3}} + 2 \right) \Bigg] \end{aligned} \tag{73}$$

The following abbreviation is introduced:

$$\overline{F}_0 = \frac{3 \cdot k_0}{K \cdot v} F_T^H \cdot e^{\left(\frac{F_0}{F_T^H} \right)^{\frac{1}{3}}} \cdot \left(\left(\frac{F_0}{F_T^H} \right)^{\frac{2}{3}} - 2 \cdot \left(\frac{F_0}{F_T^H} \right)^{\frac{1}{3}} + 2 \right) . \tag{74}$$

Eventually it follows for the total probability

$$P(F) = \exp\left[-\frac{3 \cdot k_0}{K \cdot v} F_T^H \cdot e^{\left(\frac{F}{F_T^H}\right)^{\frac{1}{3}}} \cdot \left(\left(\frac{F}{F_T^H}\right)^{\frac{2}{3}} - 2 \cdot \left(\frac{F}{F_T^H}\right)^{\frac{1}{3}} + 2 \right) + \overline{F}_0 \right]. \tag{75}$$

Eq. (48) relates the derivative of the total probability P to the probability P_{jump} for a break-through at a given force:

$$P_{jump}(F) = \frac{k_0}{K \cdot v} \cdot \exp\left[-\frac{3 \cdot k_0}{K \cdot v} \cdot F_T^H \cdot e^{\left(\frac{F}{F_T^H}\right)^{\frac{1}{3}}} \cdot \left(\left(\frac{F}{F_T^H}\right)^{\frac{2}{3}} - 2 \cdot \left(\frac{F}{F_T^H}\right)^{\frac{1}{3}} + 2 \right) + \overline{F}_0 + \left(\frac{F}{F_T^H}\right)^{\frac{1}{3}} \right] \tag{76}$$

In order to calculate the average break-through force, the integral from eq. (41) should be solved. Analytically, this is impossible. Therefore it is approximated that $P(F_{av})$=0.5. Calculating this condition for eq. (75) leads to

$$\ln 0.5 = -\frac{3 \cdot k_0}{K \cdot v} F_T^H \cdot e^{\left(\frac{F}{F_T^H}\right)^{\frac{1}{3}}} \cdot \left(\left(\frac{F}{F_T^H}\right)^{\frac{2}{3}} - 2 \cdot \left(\frac{F}{F_T^H}\right)^{\frac{1}{3}} + 2 \right) + \overline{F}_0 . \tag{77}$$

This equation contains the three unknown parameters k_0, F_T, and $\overline{F}_0$. F_T is related to αV while $\overline{F}_0$ contains the threshold force F_0. Eq. (77) cannot be solved analytically. Hence, the unknown k_0, αV and F_0 can only be extracted numerically. For simplicity it is assumed that F_0=0 (i.e. $\overline{F}_0 = \frac{6 \cdot k_0}{K \cdot v} F_T^H$). This assumption will be justified *a posteriori* by the measurements. Eq. (77) can be rearranged to give

$$k_0 = \frac{\ln 0.5 \cdot K \cdot v}{3 \cdot F_T^H \cdot \left(-\left(\frac{F_{av}}{F_T^H}\right)^{\frac{2}{3}} \cdot e^{\left(\frac{F_{av}}{F_T^H}\right)^{\frac{1}{3}}} + 2 \cdot \left(\frac{F_{av}}{F_T^H}\right)^{\frac{1}{3}} \cdot e^{\left(\frac{F_{av}}{F_T^H}\right)^{\frac{1}{3}}} - 2 \cdot e^{\left(\frac{F_{av}}{F_T^H}\right)^{\frac{1}{3}}} + 2 \right)}. \tag{78}$$

Values for v and F_{av} from the measurement of the average break-through forces in dependence on the velocity can be inserted. This generates a pair of two equations that

can be solved graphically or numerically as described for the solid foundation nucleation model.

The retract

The Hertz semi sphere nucleation model does not describe the situation of the cantilever during the retract properly. The AFM tip adheres tightly to the substrate until it detaches. Again, the flat stamp model is used to describe the retract.

Numerical analysis: Conclusions from the models

In this section the previously derived results shall be analyzed. The first issue is to compare the results of the flat stamp nucleation model, the Hertz semi sphere nucleation model, and the solid foundation nucleation model. Then I investigate how the tip size and the elastic modulus affect the break-through forces in the Hertz semi sphere and the elastic foundation nucleation model. The last issue is to validate all approximations that have been made in the models.

Break-through forces in the various models

The break-through force in the flat stamp, the solid foundation, and the Hertz semi sphere nucleation model were calculated for several parameters k_0, $\alpha V/A$ (flat stamp), αV (Hertz semi sphere, solid foundation), and velocities v. Figure 19 shows the results. The parameters of the models are chosen such that the break-through forces are approximately in the same range. All models exhibit common features. Keeping all other parameters constant, the break-through force increases with increasing approach velocity, decreasing activated volume and decreasing hole formation rate k_0. All dependencies can be intuitively understood.

Break-through force increases with increasing approach velocity. The break-through is modelled as a thermally activated process; that means that at a given load it takes a certain time until a thermal fluctuation carries the AFM tip through an adsorbed lipid bilayer. If this load is constantly increased, the waiting time continuously decreases. However, taking the point of view of applied load, possibly one has to wait very long until a break-through occurs if the load is increased very slowly but eventually this will happen. If the load is increased very quickly, the waiting time is strongly reduced but the load at which the break-through takes place is much higher than in the previous case. Therefore the break-through force increases with increasing tip velocity.

Break-through force increases with decreasing activated volume. In a nucleation model the activated volume is the volume of a hole that forms under the tip. The bigger this hole is, the bigger is the probability that the AFM tip breaks through the bilayer.

Break-through force increases with decreasing hole formation rate. A break-through occurs if a thermal fluctuation in the lipid bilayer leads to a hole in the bilayer exactly under the tip that is sufficiently big to allow the penetration of the tip. The probability for such an event increases for larger hole formation rates.

All models can reproduce the same dependencies of the break-through force on the approach velocity. In Figure 20 three curves are plotted that show the dependence of the break-through force on the approach velocity of the tip for the flat stamp, the Hertz semi sphere, and the solid foundation nucleation model. No threshold force was assumed in all cases and the parameters for the individual models were chosen manually such to reproduce the same curve. The curves are essentially undistinguishable which shows that all three models are able to describe the break-through force as a function of tip velocity. However, the parameters that are used in the various models are fairly different. For the flat stamp model one gets k_0=1.03·10^{-7} s^{-1} and $\alpha V/A$= 1.26 nm^3. In the solid foundation model one obtains k_0=8.1·10^{-17} s^{-1} and αV= 1.92 nm^3 while for the Hertz semi sphere model k_0=7.3·10^{-26} s^{-1} and αV= 3.25 nm^3.

Flat stamp model

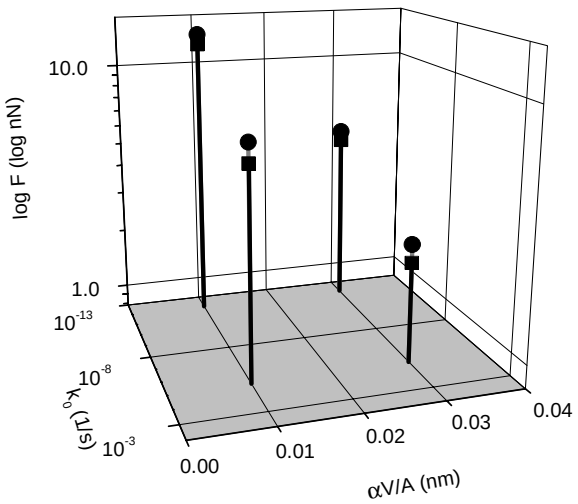

Hertz semi sphere model

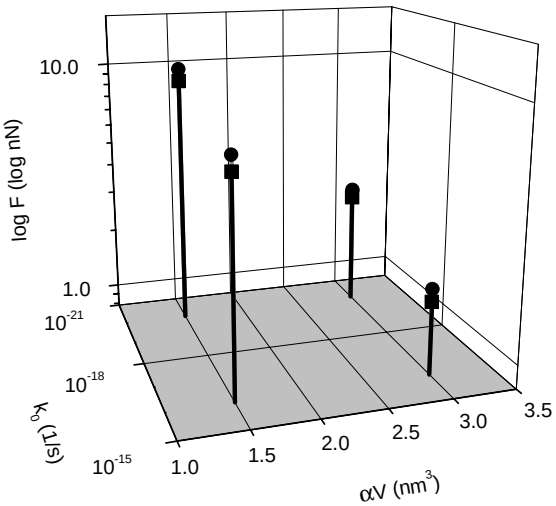

Solid foundation model

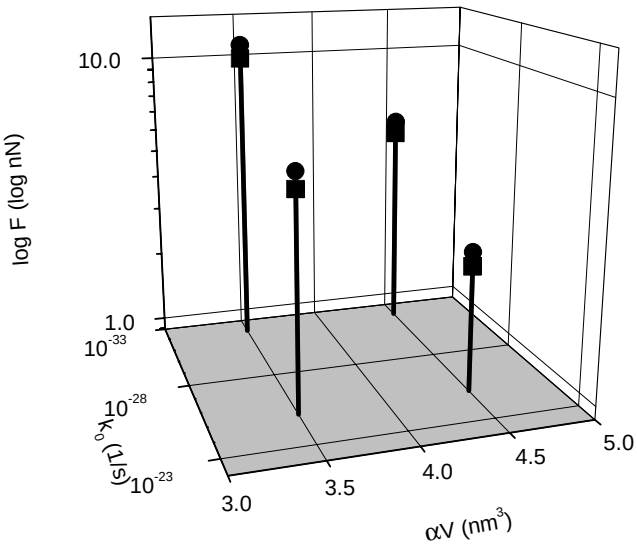

Figure 19. Breakthrough forces for different values of k_0 and $\alpha V/A$ and αV for the flat stamp, the Hertz semi sphere model, and the elastic foundation model, respectively. The forces are calculated for two different approach velocities, v=4 µm/s (circles) and v=0.2 µm/s (squares). F_0 is set equal to 0, E=1 N/m^2, K=0.1 N/m, R=40 nm, and $k_BT=4\cdot10^{-21}$J.

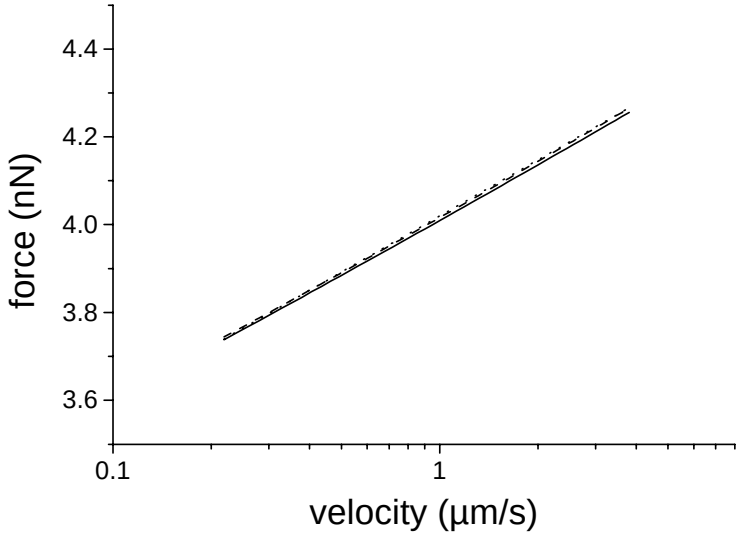

Figure 20. Break-through force in dependence of the approach velocity. The parameters for the curves were chosen such to give a match that is as close as possible. For the individual models the following parameters were chosen: Flat stamp (dotted line): $k_0=1.03\cdot10^{-7}$ s^{-1} and $\alpha V/A= 2.17\cdot10^{-11}$ nm; Hertz semi sphere (dashed line): $k_0=6.4\cdot10^{-26}$ s^{-1} and $\alpha V = 3.25\cdot10^{-11}$ nm; Solid foundation (solid line): $k_0=8.1\cdot10^{-17}$ s^{-1} and $\alpha V = 1.92$ nm^3.

Selection of an appropriate model

Summarizing, the three models can reproduce similar dependences of the break-through force on the approach velocity of the tip. The parameters for the hopping rate and the activated volume, however, depend sensitively on the chosen model.

From a formal point of view a main difference between the proposed models is the power law that governs the dependence of the maximum pressure under the tip on the applied force. For the flat stamp nucleation model $\Delta p_{max}=const.\cdot F$, for the solid foundation nucleation model $\Delta p_{max}=const.\cdot F^{1/2}$, and for the Hertz semi sphere nucleation model $\Delta p_{max}=const.\cdot F^{1/3}$. The calculations show that decreasing the exponent decreases the hopping rate and increases the activated volume.

It remains the question which model shall be used in order to describe the measurements of this work. The flat stamp nucleation model makes the unrealistic assumption that the tip is rectangular. Therefore it is not appropriate to account for the experiments. Nevertheless it is valuable because it is the only model that can be treated analytically.

The dependence of the applied force on the deformation of the sample is too similar for the Hertz semi sphere nucleation model and the elastic foundation nucleation model to discriminate between them. However, from a physical point of view, the solid founda-

tion nucleation model is appropriate for measurements with standard AFM tips on soft adsorbed layers. The Hertz semi sphere nucleation model is only valid when the deformation of the liquid layer is small compared to the total thickness of the adsorbed layer. This is not the case for most experiments. Therefore, throughout this work only the solid foundation nucleation model will be used in order to obtain quantitative parameters from the measurements.

Influence of the tip shape on the models

Both in the Hertz semi sphere nucleation model and in the elastic foundation nucleation model appears the ratio between elastic modulus and tip radius, E/R, that consequently both must be known.

One important parameter is the elastic modulus that has to be determined individually for every experiment. It is experimentally accessible via the force curves as described above once an appropriate model has been chosen.

As mentioned above, the tip shape is an experimental parameter that is hardly accessible with our experimental means. Therefore it is important to know whether this poorly known parameter has a significant influence on the break-through force. The dependence of the break-through force on the approach velocity of the tip has been calculated for two identical sets of parameters k_0 and αV but different radii. The graphs shown in Figure 21 are calculated for R=40 nm and R=60 nm. They show a significant difference between the average break-through forces of about one order of magnitude. For a radius of 60 nm the break-through force in the Hertz semi sphere nucleation model approximately doubles while in the solid foundation nucleation model the break-through force is approximately 50% larger for the bigger radius.

The result shows that the calculation of the activated volume and the hole formation rate are affected by a certain error that decreases the more precise the tip shape is known.

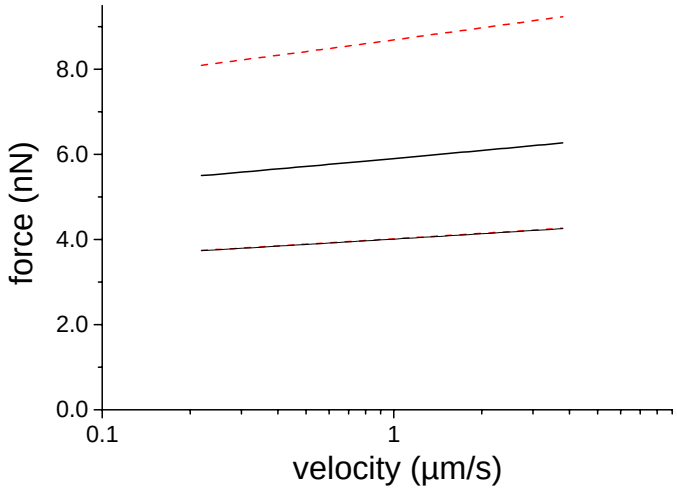

Figure 21. Break-through forces in the Hertz semi sphere nucleation model (dashed curve) and in the elastic foundation nucleationmodel (solid curve) for two different radii. The two lower curves are calculated with both models using the same parameters as above and a radius of 40 nm. The two upper curves are calculated for a radius of 60 nm.

Justification of the approximations in the models

For the various models several approximations were made that have to be justified. For this purpose the dependence of the break-through force on the approach velocity of the tip has been calculated numerically for each model by use of the exact eqs. (41) and (47) for a given set of parameters k_0 and αV. From the calculated graph the initial parameters have then been reobtained by the approximate formulas. The approximation is considered as valid if the initial parameters and the reobtained ones do no deviate by more than 5% from each other.

In all cases the threshold force F_0 has been set to zero. A threshold force larger than zero would cause an increase of the break-through force that is lower at low velocities than at higher ones (cf. Figure 17). Such a behaviour was never found in the experiments so that the assumption F_0=0 N is justified.

For each model the same experimental parameters have been used in order to make the results comparable. The elastic modulus of the adsorbed layer is E=1 GPa, sphere and substrate are taken as completely rigid. The spring constant is K=0.1 N/m, the tip radius 40 nm. In all calculations the temperature is 300 K so that k_BT=4.0·10^{-21} J. The activated volume and the hole formation rate are different for each model. They are chosen such that the average break-through forces F_{av} depend approximately in the same way on the approach velocities v for all models.

flat stamp nucleation model

In the flat stamp nucleation model two approximations have been proposed. The first is not to calculate the integral from eq. (47) in order to obtain the average break-through force but to get it from the condition P=0.5 that eventually results in eq. (50). The second approximation is to fit the dependence of the break-through force F_{av} of the tip approach velocity v not with eq. (50) but with $F_{av}=a+b\cdot\log v$, where a and b are fitting parameters that can be computed via eqs. (55) and (56).

For the activated volume $\alpha V/A=2.17\cdot10^{-11}$ m is chosen and the hopping rate is set to be $k_0=1.03\cdot10^{-7}$ s^{-1}. Subsequently a best fit to this function was made with eq. (50). The best fit is $F_{av}=0.183\cdot10^{-9}\cdot\ln(3.5\cdot10^{15}\cdot v+1)$. From the fit the parameters $k_0=1.08\cdot10^{-7}$ s^{-1} and $\alpha V/A=2.2\cdot10^{-11}$ m were recalculated. This result shows that with the approximation P(F_{av})=0.5 the error is negligible.

In order to check the second approximation a logarithmical fit was made with eq. (53). The result is $F_{av}=6.57\cdot10^{-9}$ N+$4.24\cdot10^{-10}$ N$\cdot\log v$ and the corresponding parameters are calculated to be k_0=70 s^{-1} and $\alpha V/A=2.17\cdot10^{-11}$ m. Hence, in this approximation the activated volume is exactly reproduced while the hopping rate is largely overestimated.

The area A over which the pressure is acting can be estimated either by use of the Hertz semi sphere model or by the solid foundation model. If the above-mentioned values for the elastic modulus of $1\cdot10^9$ GPa and a radius of the tip of 40 nm are assumed, in the Hertz semi sphere model the contact area is

$$(79) \qquad A=\pi a^2=\pi\cdot\left(\frac{R\cdot F}{4/3\cdot E}\right)^{\frac{2}{3}}=56\ nm^2.$$

In the solid foundation model one obtains

$$(80) \qquad A=\pi a^2=2\cdot\left(\frac{\pi\cdot R\cdot h\cdot F}{E}\right)^{\frac{1}{2}}=61\ nm^2.$$

An average value of 58 nm^2 will be used. Then the activated volume can be calculated to be $\alpha V=\alpha V/A\cdot A=2.17\cdot10^{-11}\cdot58\cdot10^{-18}$ m^3=$1.26\cdot10^{-27}$ m^3.

Summarizing, a fit with eq. (50) yields good results for the parameters k_0 and αV but the approximation of eq. (53) is too coarse to be applicable.

Hertz semi sphere nucleation model

The approximation that has been proposed for the Hertz semi sphere model is to avoid the integration eq. (47) and to calculate the average break-through force from the condition P=0.5 instead. The break-through force in dependence of the approach velocity was calculated with the initial parameters k_0=7.3·10^{-26} s^{-1} and αV=3.25 nm^3. By inserting two calculated values for F_{av} and v in the eq. (78) two equations were generated that were solved numerically for k_0 and αV. The results were k_0=7.29·10^{-26} s^{-1} and αV=3.245 nm^3.

Thus the error of the approximation P=0.5 is negligible for the computation of k_0 and αV in the Hertz semi sphere model.

Solid foundation nucleation model

In order to check the precision of this approximation P=0.5 the break-through force was calculated numerically with eq. (47) for two sets of parameters to obtain two curves for the break-through forces in dependence on the velocity. For the first curve the parameters were k_0=1.0·10^{-16} s^{-1}, αV=1.93 nm^3, and k_0=0.01 s^{-1} and αV=0.5 nm^3 for the second. The height h=4 nm was kept constant.

Figure 22 shows that the first curve coincides well with the curves for the other two models while a second one is steeper. Recalculating k_0 and αV numerically yields k_0=8.1·10^{-17} s^{-1} and αV=1.92 nm^3 for the first curve and k_0=1.2·10^{-8} s^{-1} and αV=5.7 nm^3 for the second. While the error for the first set of parameters is negligible, the second set is not by far reproduced.

The result shows that the error depends on the slope of the break-through forces in dependence on the velocity. The error increases for larger slopes. If the recalculation exhibits so large an error the experimenter must vary the parameters until satisfactory fit between calculations and experiments is obtained.

Discussion of the hole formation rate k_0

The hole formation rate k_0 is introduced as the rate at which holes form spontaneously in the bilayer. Consider

$$(81) \qquad k_0 = \frac{k_B T}{h} \cdot e^{-\frac{G_0^*}{k_B T}}.$$

Evaluating the prefactor at 300 K gives

$$(82) \qquad \frac{k_B T}{h} = 6 \cdot 10^{12}\, s^{-1}.$$

The activation free enthalpy G_0^* refers to the nucleation theory for hole formation in liquid layers by Persson and Tosatti (Persson and Tosatti 1994). The free enthalpy for the formation of a circular hole in a two-dimensional liquid layer is given by two contributions.

1. The line tension Γ times the length of the hole with radius R accounts for the energy necessary for the creation of a free line in the film where the bonds of the molecules cannot be saturated any more.

2. The area of the hole times the spreading coefficient $S=\gamma_s-\gamma_{bs}-\gamma_{bv}$ accounts for the destruction of the layer-solid and the layer-liquid interfaces, and the creation of a solid-liquid interface. Here, γ_s, γ_{bs}, γ_{bv} denote the solid-liquid, the layer-solid and the layer-liquid interfacial energies, respectively.

Summing up the two contributions finally leads to

$$(83) \qquad G_0^* = 2\pi R \cdot \Gamma + \pi R^2 \cdot S\,.$$

Eq. (83) can be used to estimate G_0^*. The calculation is intended as a very rough estimate of the hopping rate because the exact numerical values for the parameters depend on the individual system and are not known in many cases. According to the publication of Persson and Tosatti a spreading coefficient S=0.03 J/m^2 is used while the line tension is 10^{-11} J/m. The radius of the hole is a critical parameter that is arbitrarily set to 1 nm, the approximate radius of a single molecule in the layer. Inserting these values in eq. (81) yields

$$(84) \qquad k_0 \cong 6 \cdot 10^{12}\, s^{-1} \cdot e^{-\frac{16 \cdot 10^{-20}}{4 \cdot 10^{-21}}} \cong 2 \cdot 10^{-5}\, s^{-1}.$$

Taking for the radius of a hole the double value, i.e. 2 nm, one obtains:

$$(85) \qquad k_0 \cong 6 \cdot 10^{12}\, s^{-1} \cdot e^{-\frac{50 \cdot 10^{-20}}{4 \cdot 10^{-21}}} \cong 3 \cdot 10^{-42}\, s^{-1}.$$

These values indicate that the hole formation rate is small and that it may vary over many orders of magnitude, depending on the size of the hole in the bilayer. However,

the prefactor k_BT/h is not strictly applicable and therefore all results represent only a first estimate.

Scope of the theory

The objective of this work was to clear the break-through for the special case of lipid bilayers. Therefore the theory has been initially derived for this system. However, break-throughs are observed in many other cases, e.g. in *n*-alcohols that were investigated in this work. The theory never makes use of the peculiar properties of lipid bilayers so that it can be applied to the other systems, too. Always when the average break-through force depends on the approach velocity then the molecules have to overcome an activation barrier larger than k_BT before they can change their places in order to form a hole. Therefore the method opens a way to discriminate between systems with liquid *layers*, in which the molecules are bound among each other and systems in which the forces between the molecules are so weak that they can move almost freely.

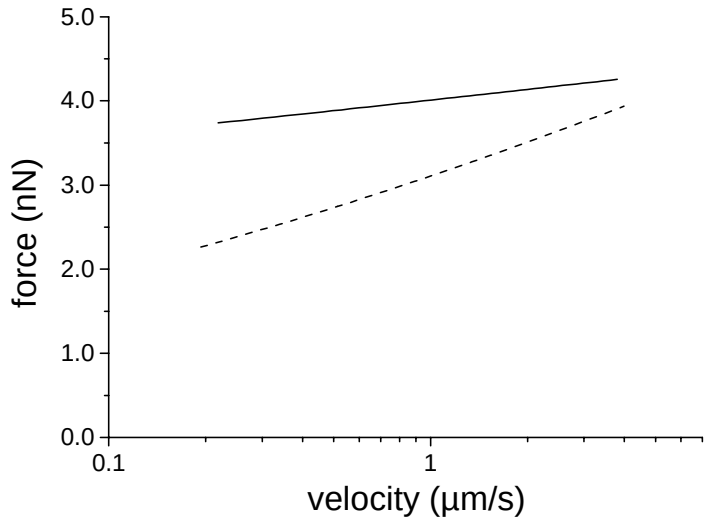

Figure 22. Simulated break-through force in dependence of the approach velocity of the AFM tip in the solid foundation model. For both curves R=40 nm, $k_BT=4\cdot10^{-21}$J, $E=1\cdot10^{-9}$ N/m^2, K=0.1 N/m. Activated volume and hopping rate are set as follows: $\alpha V=1.92$ nm^3, $k0=8.1\cdot10^{-17}$ s^{-1} (solid line) and $k_0=0.01$ s^{-1} and $\alpha V=0.5$ nm^3 (dashed curve).

5. Tip Penetration through Lipid Bilayers

Motivation

In the study of solid supported lipid bilayers the atomic force microscope has become a useful tool. By imaging lipid bilayers in an aqueous medium their molecular structure as well as their defects have been studied (Weisenhorn, Egger et al. 1991; Zasadzinski, Helm et al. 1991; Hui 1995; Dufrene, Boland et al. 1998; Viitala and Peltonen 1999; Schneider, Dufrene et al. 2000; Muresan and Lee 2001). When force curves are measured on lipid bilayers often a jump of the tip is observed once a certain threshold force has been exceeded. Several authors have described jumps on different types of bilayers (Rädler, Radmacher et al. 1994; Dufrene, Boland et al. 1998; Müller, Butt et al. 2000; Schneider, Dufrene et al. 2000). However, no model has been proposed that describes the break-through quantitatively. In this work the break-through is interpreted as a penetration of the AFM tip through the lipid bilayer. This can be done quantitatively in the framework of the above theory.

For the experiments lipid supported bilayers of dioleoyltrimethylammoniumpropane chloride (DOTAP) and dioleoylphosphatidylserine (DOPS), both on mica, were used as model systems (Figure 23). DOTAP is commonly used for transfection of negatively charged molecules like DNA or RNA into cells. DOPS is one of the phospholipids that can be found in biological systems.

a

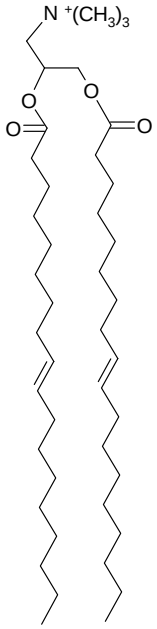

b

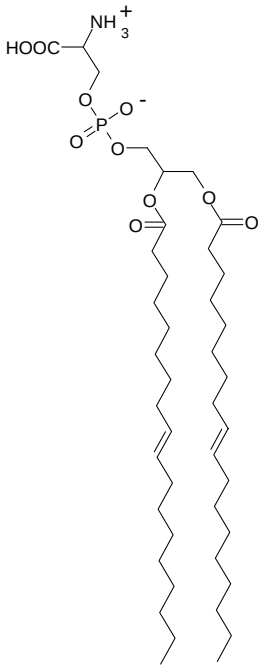

Figure 23. Structure of a) dioleoyltrimethylammoniumpropane, b) dioleoylphosphatidyl-serine

Experimental

All chemicals were of analytical grade and were used without further treatment. DOTAP was purchased from Aldrich, Steinheim, Germany and from AvantiLipids, Alabaster (AL), USA. The latter was also the supplier for DOPS. Providers of the other materials were Merck, Darmstadt, Germany (Chloroform, Potassium Chloride, Potassium Hydroxide), Fluka, Neu-Ulm, Germany (Sodium Chloride), and Plano GmbH, Wetzlar, Germany (Muscovite Mica). Measurements were carried out with the commercial AFM (NanoScope III, Digital Instruments, Santa Barbara, CA) that was equipped with a liquid cell. The cell is schematically shown in Figure 24. The chip with cantilever and tip is clamped to the bottom side of the glass cell. It is positioned in the center of a circular pit into which a silicon O-ring is put that seals the glass cell together with the sample. The gap between glass cell and sample can be filled with liquid.

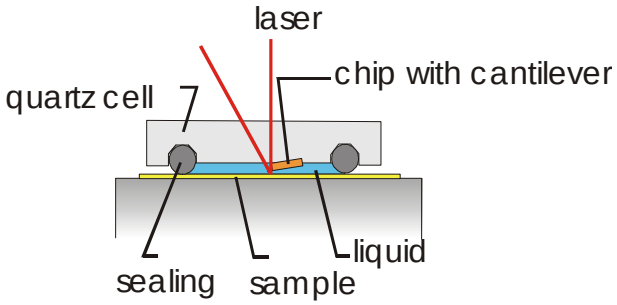

Figure 24. Schematic view of the glass cell for measurements in liquids

Silicon nitride cantilevers (Digital Instruments, CA, length 200 µm or 100 µm, width 40 µm, estimated thickness 0.6 µm) were used. The tip was either bare silicon nitride or functionalized with mercapto-undecanol or mercapto-undecanoic acid. In order to functionalize the tips, they were first covered with a 3 nm thick layer of Chromium and subsequently with a 20 nm thick layer of gold. Then the freshly prepared cantilevers were immersed into a 1 mM solution of the respective thiol in ethanol for at least 6 hours in a closed beaker. Thiols were purchased from Aldrich, Steinheim, Germany, and were used without further purification. The radius of the tip curvature was measured individually for every tip after use. Both methods that are described in chapter 3 were applied, i.e. the measurement in a transmission electron microscope and the measurement with a spike.

Cantilever spring constants were individually determined by moving them against a reference cantilever, yielding values in the range of 0.07-0.1 N/m for the long cantilevers and 0.23-0.28 N/m for the short one. We calibrated the AFM scanner in the vertical direction as described by Jaschke and Butt (Jaschke 1995).

At room temperature DOTAP and DOPS form vesicles in aqueous solution after sonification. The vesicles are in a liquid state and by fusion they spontaneously form bilayers on mica. Experimentally, lipid vesicles for adsorption on mica were prepared as follows: The lipids were first dissolved in chloroform. Then this solvent was evaporated under a constant stream of N_2 or by applying a vacuum of approximately 100 mbar. A buffer solution of 150 mM NaCl and 5 mM KH_2PO_4 that was titrated to pH 7.4 with 1 M KOH was added to the obtained lipid film to produce a 5 mg/ml suspension which subsequently was thoroughly sonicated (G112SP1T sonicator (Laboratory Supplies Co., Hicksville, NY) until the suspension became opalescent.

Mica was freshly cleaved and mounted onto the AFM scanner. Immediately after cleavage a drop of buffer solution was placed on the mica in order to prevent adsorption of contaminants on the surface. Then, the AFM head with liquid cell, O-ring, and tip was mounted. As quickly as possible 50 µl of the vesicle solution were pipetted into the cell. The solution has been heated to 50°C for 1 minute before. After 30 min adsorption time the cell was rinsed with approximately 1 ml buffer solution to remove vesicles that did not adsorb to the mica substrate. 10 min later the measurement started. Before each measurement an image of the lipid bilayer was taken in order to check the bilayer quality. After preparation of a bilayer force curves have been measured always on the same point of the bilayer. Force curves are collected repeatedly, typically 20 or 50 for six approach velocities. Each deflection versus piezo movement curve was transformed into a force-distance curve with the self-made programs *forcecurves2,* programmed in *C for virtual instrumentation* (CVI, National Instruments, Austin, Texas). The ensemble of all force curves at a given velocity is called *velocity series*. After recording 5 or 6 velocity series at different approach velocities the AFM was unmounted. All force curves that were measured during this session are termed *multivelocity series*. The glass cell was rinsed with water and isopropanol and dried under a nitrogen stream. The cantilever was rinsed under water and stored in a dry place. No cantilever was used twice if not explicitly noted otherwise.

Results and Discussion

This section is divided in five parts. In the first part the general methods for the analysis of the force curves is presented. In the second part the evaluation of histograms of the break-through is shown. Thereafter the specific results for DOTAP and DOPS are presented. In the fifth part the measurements are discussed and compared.

Analysis of the force curves

A typical force curve is shown in Figure 25. Three different forces are relevant in order to describe the approach part of each of the measured force curves.

Up to the break-through, all curves of the multivelocity series contain the same information about these forces. Figure 26 shows two force curves (taken from the multivelocity series labelled DOTAP1), one taken at 0.2 µm/s the other one taken at 2 µm/s. Both curves exhibit identical surface forces. This shows that velocity dependent effects,

like hydrodynamics, can be neglected for the range of velocities applied in these experiments.

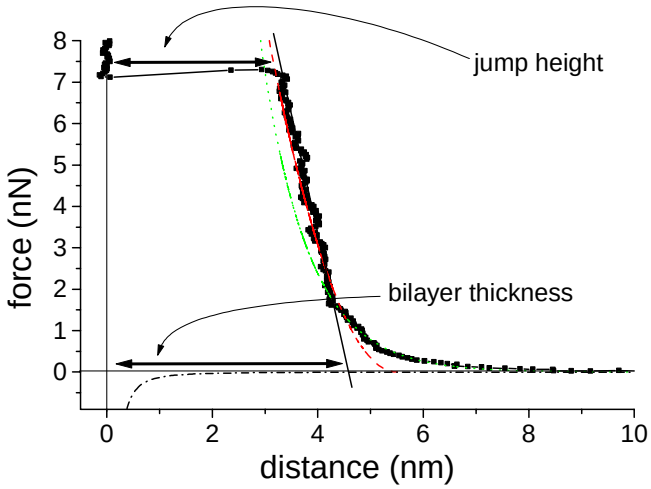

Figure 25. A force curve on a lipid bilayer can be fitted by three types of forces. As an example a force curve on DOTAP is shown. In the region between 4.5 and 10 nm the electrostatic repulsion (dotted curve) dominates the force between tip and bilayer. At smaller distances the contact force according to the solid foundation model (dashed curve) describes the force. The van der Waals force (dash dot) plays a role for distances smaller than 2 nm.

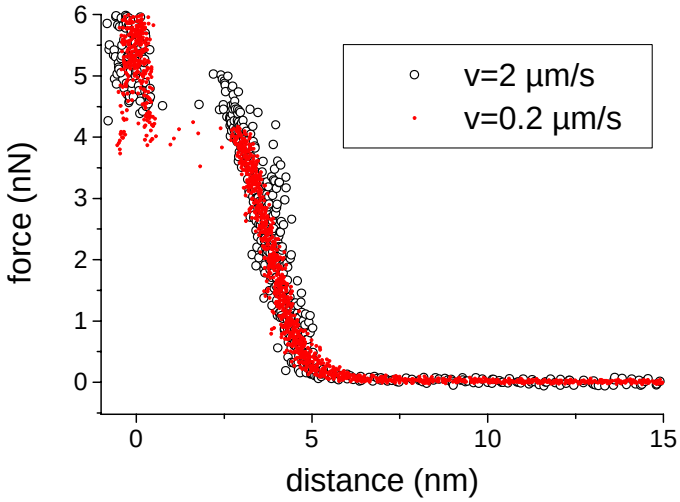

Figure 26. The graph shows two force curves on DOTAP. Each force curve has been averaged form at least 5 individual force curves. Solid circles: 0.2 µm/s. Open circles: 2 µm/s.

The fitting procedure is demonstrated in the sample curve in Figure 25. The force with the longest range that acts between an AFM tip and a lipid bilayer is the electrostatic

force that obeys the law $F \sim e^{-(d-H)/\kappa}$ with the Debye length $1/\kappa$ and H, the distance by which the exponential function is shifted out of the origin. The parameter H is roughly given by the height of the bilayer. For a 150 mM electrolyte solution that is used throughout the experiments the theoretical Debye length is 0.78 nm.

In all measurements on lipid bilayers the attractive van der Waals force, is not detectable during the approach of the tip to the bilayer surface. This is expected from the formula for the van der Waals force in eq. (6). Inserting an approximate value of $2 \cdot 10^{-20}$ J for the Hamaker constant A (Israelachvili 1992), p. 190, and a tip radius R of 40 nm one finds $F = -1.3 \cdot 10^{-28}/d^2$. Thus, at the surface of the bilayer at a distance of 4 nm the contribution of the mica substrate is only about 0.01 nN.

As soon as the tip is in direct contact with the bilayer the contact force comes into play. As outlined before the solid foundation model is considered the most appropriate model to describe the situation of a tip that deforms a lipid bilayer elastically. It will be exclusively employed for analysis. Thus a function of the form

$$F = \frac{\pi E R (H_{sf} - d)^2}{h} \tag{86}$$

is fitted to the increasing part of the force curve just before the break-through. H_{sf} denotes the distance by which the curve is shifted away from the origin and d is the distance of the tip from the substrate.

Note that in general apart of the contact force and the electrostatic force also other forces like the hydration force may play a role (Butt and Franz 2001). However, for the experiments presented here already the prior force models are sufficient to describe the force curves.

An important parameter for a bilayer is its thickness. It is not straightforward to deduce it from the force curves because it is not clear when the deflection of the cantilever is not due to the electrostatic repulsion any more but to the contact forces between bilayer and tip. A possibility would be to fit electrostatic and contact forces and the thickness is determined from the distance of the fits to the origin. However, the fits for the electrostatic interaction and for the contact force usually give different results. In order to obtain a well-defined thickness for each bilayer, the almost straight increase of the force before the break-through is extrapolated and the intersection with the line of zero force is taken as the thickness of the bilayer. Note that this is a mere definition without a

physical justification. It serves only to get a well-defined thickness of the bilayer that can be inserted in the solid foundation model that is close to the parameters H and H_{sf} for the electrostatic repulsion and the solid foundation model, respectively.

A second quantity that is closely related to the thickness of the bilayer is the distance over which the tip jumps when the break-through takes place, referred to as *jump height* (see Figure 25). At this point the bilayer is already compressed by the pressure that is exerted by the tip and therefore the jump height generally is smaller than the bilayer thickness. The jump height is evaluated statistically together with the break-through forces.

Histograms of break-through forces

The approach parts of the force curves show a characteristic break-through at a certain force. These break-through forces can be evaluated statistically for a velocity series, i.e. measurements done with the same cantilever on the same bilayer at the same approach velocity. The results are represented in a histogram. The height of the bars indicates the number of break-throughs in a certain force interval. The histogram is fitted by a Gaussian curve centered around the average value for the break-through force, F_{av}. The standard deviation of the Gaussian curve is denoted as ΔF.

An example is shown in Figure 27. The Histogram shows the break-through forces of 400 force-distance curves measured at a tip velocity of 2 µm/s on a bilayer of DOTAP. Such histograms were recorded for break-through forces at different tip velocities. As an example in Figure 28 two histograms for 50 measurements at two different approach velocities are shown. The underlying force measurements have been carried out on a DOPS bilayer. The figure shows that on average the break-through force increases with increasing approach velocity.

Eventually the average break-through forces of a series of measurements with the same tip on the same bilayer are plotted versus the individual approach velocity. These curves are the basis for the discussion in the subsequent chapters. According to the equations that have been derived in chapter 3 the parameters αV and k_0 can be obtained from a best fit to the function $F(v)$, the break-through force in dependence on the approach velocity.

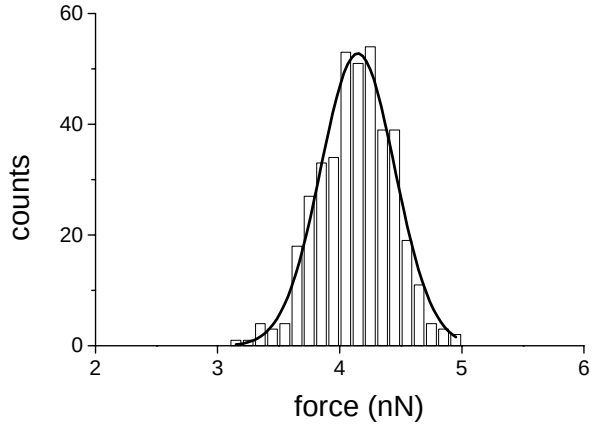

Figure 27. Histogram for the break-through forces for 400 single force curves measured on DOTAP at an approach velocity of 2 µm/s. The envelope is a Gaussian curve showing that the histogram is approximately described by this type of curve.

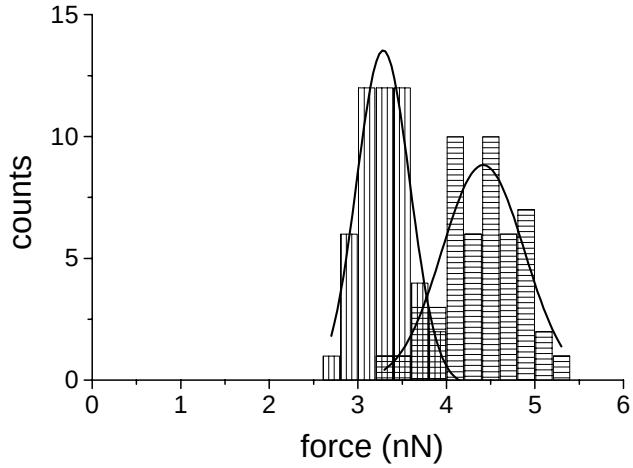

Figure 28. Histograms for break-through forces at two approach velocities. v=2 µm/s (vertically striped bars); v=12.8 µm/s (horizontally striped bars). Two Gaussian functions are fitted to the histograms (solid lines).

Results for DOTAP

Five multivelocity series have been recorded on DOTAP bilayers in electrolyte solution. They are named DOTAP1 to DOTAP5. In each multivelocity series at least one break-through occurred.

First, measurements have been made with an uncoated silicon nitride tip. They are denoted DOTAP1 to DOTAP3. The multivelocity series DOTAP4 has been recorded with a functionalized tip. It was covered with mercapto-undecanol. Four samples of each of the three multivelocity series of force curves are presented in Figure 29. In these measurements the maximal applied force was in the range from 8 nN to 17 nN. Only a part of the whole range is shown in the figures.

In all of these experiments one single break-through could be observed. The break-through force for all three multivelocity series increased with increasing approach velocity as predicted by the nucleation models.

The solid foundation nucleation model has been used to fit the data points for each multivelocity series. The diagrams together with the fits are shown in Figure 30. The activated volume and the hopping rate have been calculated by inserting two measured average break-through forces at two different velocities in eq. (67). The resulting system of two equations was solved numerically. For the fit the dependence of the break-through force versus the approach velocity has been recalculated with these parameters. The resulting values for the activated volume and the hopping rate are listed in Table 1.

The bilayer thickness was in a narrow range between 4.6 and 4.9 nm while the jump height was between 2.5 nm and 4 nm. Figure 31 shows that the jump height decreases with increasing approach velocity. The elastic moduli, according to the solid foundation model, varied between 20 and 40 MPa. The variance can be attributed to the steep increase of the force during the approach in the contact region that induces a considerable error in the fit. It was also confirmed that the long ranging exponential force increase has a decay length of about 0.8 nm so that it can be attributed solely to the electrostatic repulsion. Adhesion forces varied strongly from force curve to force curve and therefore they have not been further evaluated.

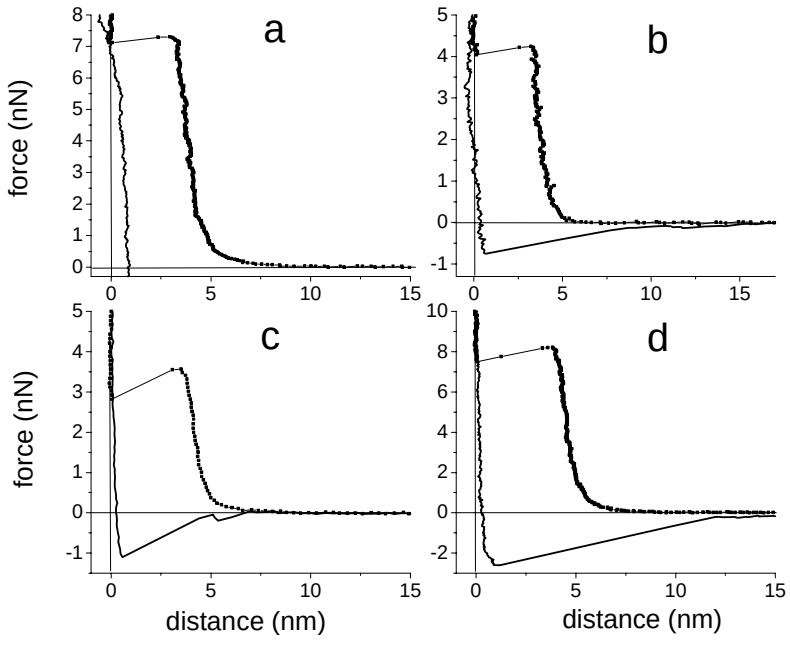

Figure 29. Four sample force curves from the multivelocity series a) DOTAP1, b) DOTAP2, c) DOTAP3, and d) DOTAP4 at an approach velocity of 0.4 µm/s taken with a bare silicon nitride tip on the same DOTAP bilayer. All curves have the same shape, demonstrating the homogeneity of the bilayer.

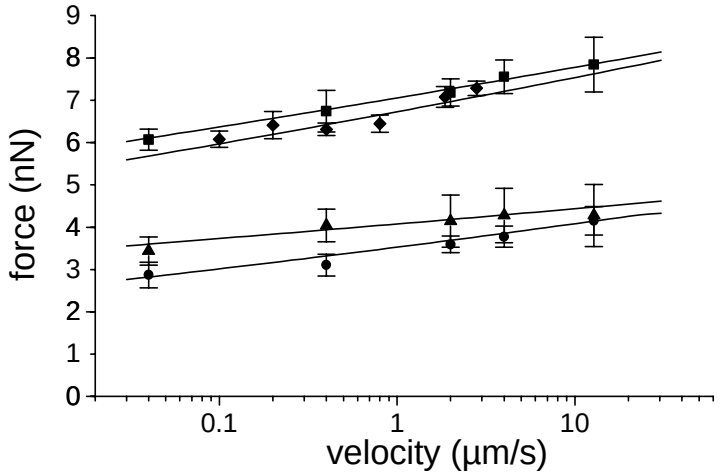

Figure 30. Break-through forces in dependence on the approach velocity of the tip. Different symbols represent different measurements. The points are fitted with the solid foundation nucleation model. The respective parameters are listed in table: DOTAP1 (squares), DOTAP2 (triangles), DOTAP3 (circles), and DOTAP4 (diamonds).

Name	Tip	Radius (nm)	Spring Constant of Cantilever	Elastic Modulus of Bilayer (MPa)	bilayer thick-ness (nm)	αV **(nm^3)**	k_0 **(1/s)**
DOTAP1	bare silicon nitride	49	0.09	40	4.6	**9.8**	**$7.2\cdot10^{-18}$**
DOTAP2	bare silicon nitride	49	0.09	40	4.9	**14.4**	**$9.9\cdot10^{-21}$**
DOTAP3	bare silicon nitride	51	0.28	20	4.6	**11.9**	**$2.0\cdot10^{-10}$**
DOTAP4	OH-terminated thiol	23	0.23	50	5.1	**5.1**	**$1.2\cdot10^{-14}$**
DOTAP5, low jump	bare silicon nitride	60	0.24	40	4.6	**7.3**	**$1.0\cdot10^{-11}$**
DOTAP5, high jump	bare silicon nitride	60	0.24	not measured	1.9*	**9.4**	**$6.3\cdot10^{-34}$**

* The height was measured as distance between the nearest points at the starting point and at the end point of the jump because the bilayer thickness could not be determined

Table 1. Parameters that reproduce the break-through forces in dependence of the approach velocity in Figure 30.

In spite of the good fit between experimentally obtained and theoretically calculated break-through forces, the values for the break-through forces vary strongly between the different multivelocity series. This means that with identical preparation the bilayers behave differently. This observation raised the questions whether the bilayers are spatially homogeneous and if the break-through forces change in time.

In order to verify the spatial homogeneity three series of measurements at three different positions of the same lipid bilayer were made at distances of at least 1.4 µm from each other. The group of three individual multivelocity series is labelled DOTAP4. For this series the AFM tip has been functionalized with mercapto-undecanol. The functionalization guarantees homogeneous and well-defined conditions on the tip surface that comes into contact with the lipid bilayer. Figure 32 shows the dependences of the average break-through forces on the approach velocity for three multivelocity series from different positions on the same bilayer, recorded with the same tip. The curves closely resemble each other. It was verified that the elastic modulus and the jump height are the same for all three curves. These findings demonstrate that the DOTAP bilayer is spatially homogeneous. Note that the average break-through forces of DOTAP4 coincide very well with those of DOTAP2 that has been obtained with an ordinary unfunctionalized tip. The other series with a functionalized tip, DOTAP5 which is discussed later, exhibits break-through forces that are also in the same range.

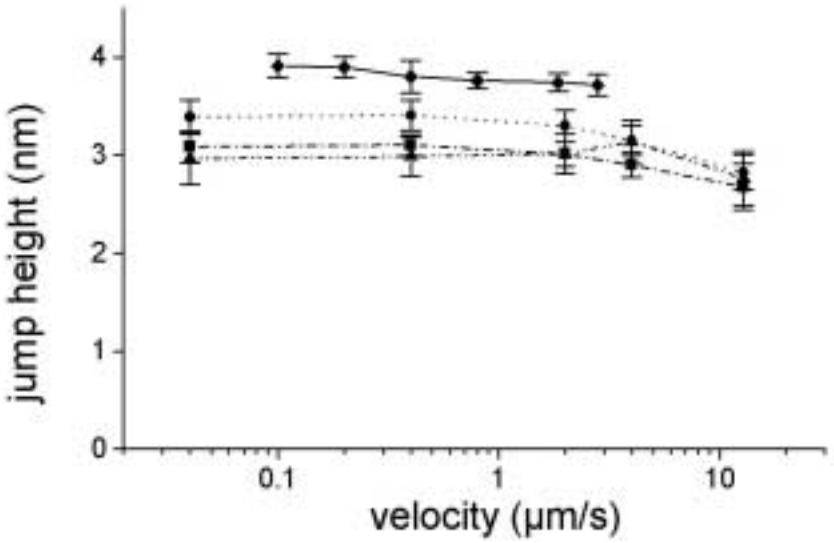

Figure 31. Jump heights in dependence on the approach velocity of the tip. Different symbols represent different measurements: DOTAP1 (squares), DOTAP2 (triangles), DOTAP3 (circles), and DOTAP4 (diamonds).

The temporal behavior of the DOTAP bilayers has been elucidated by waiting 2 hours between the measurement of two velocity series from the series DOTAP3, taken at the same velocity of 0.2 µm/s. The two histograms and two representative force curves are shown in Figure 33. The histograms demonstrate that the average break-through force increases by approximately 10 % after 2 hours. This increase indicates that the bilayers undergo slight changes in time. The shape of the force curves before the break-through remains unchanged.

The experiments for the series DOTAP1 to DOTAP4 were carried out in such a way that the maximal force exerted on the bilayer was about 17 nN. In order to achieve higher maximal forces the force curves were recorded with a cantilever with the highest available spring constant (0.24 N/m). It was pushed against the mica substrate until a force of 30 nN was reached. In Figure 34a a typical force curve of this multivelocity series, labelled DOTAP5, is shown. Generally, the use of cantilevers with a high spring constant comes at the expense of a reduced sensitivity. Additionally, at high deflections the relation between the deflection of the cantilever and the position of the laser beam on the photosensitive diode ceases to be linear. The measurement of this multivelocity series revealed a second break-through at about 25 nN. In Figure 34b the relation between average forces of the two break-throughs versus the approach velocity is plotted. Both curves follow the behaviour predicted by the elastic foundation nucleation model and the average break-through forces for both break-throughs increase with increasing approach velocity. Parameters for the activated volume and the hole formation rate could be determined and the fitted curves are added to Figure 34b.

When the tip is pulled back from the substrate always adhesion of the tip is observed. This is attributed to the van der Waals attraction that becomes very large at small distances. No further evaluation of the adhesion force has been made.

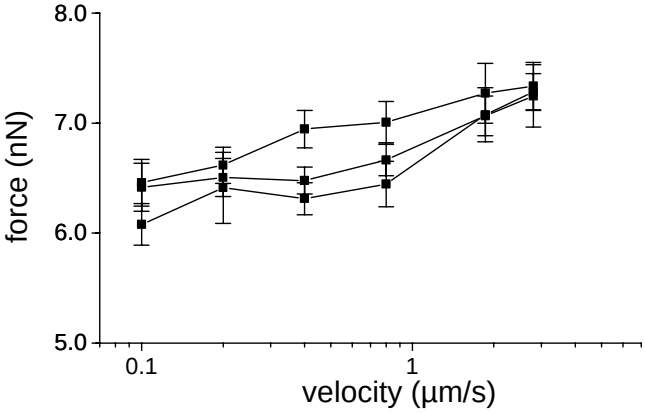

Figure 32. Average break-through forces for three mutivelocity series that were recorded on the same bilayer under identical conditions. The three multivelocity series stem from three different positions on the bilayer. The three series together are labelled DOTAP4.

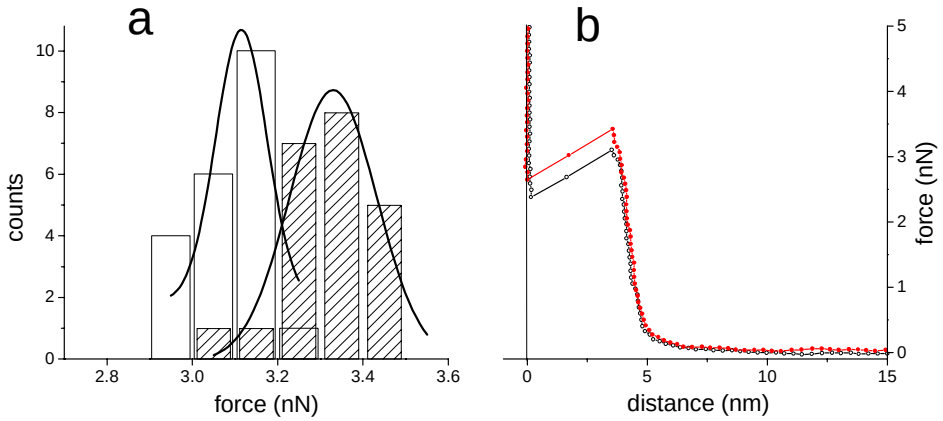

Figure 33. Histogram of break-through forces and two representative force curves measured at t=0 h (hollow bars, open circles) and t=2 h (hatched bars, solid circles). The measurements were made for the series DOTAP3 at 0.2 µm/s. The histograms are fitted by a Gaussian bell curve. The break-through forces increase after 2 hours.

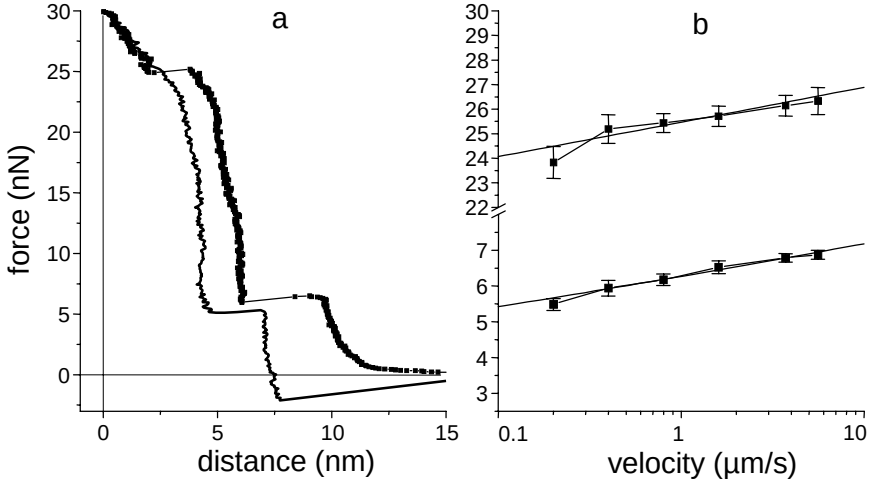

Figure 34. Multivelocity series DOTAP5 a) Typical force curve with a maximal applied force of 30 nN. Two break-throughs are discernible. The curve shows poor linearity for forces higher than about 15 nN. b) Dependence of the average break-through forces on the approach velocity for both break-throughs. The data points are fitted with the elastic foundation nucleation model. The parameters are listed in Table 1.

Results for DOPS

The results for the multivelocity series on bilayers of DOPS splitted into two groups. The multivelocity series of the first group, termed DOPS1 to DOPS3, exhibited one single break-through. Sample curves are shown in Figure 35. A second group of measurements, labelled DOPS4 to DOPS7, exhibited two break-throughs. Samples are shown in Figure 36.

The break-through force for all multivelocity series, independent whether they belong to the series with a single break-through, DOPS1 to DOPS 3, or to the series with several break-throughs, DOPS 4 to DOPS7, increased with increasing approach velocity as predicted by the nucleation models. This is shown in Figure 37 and Figure 38. The solid foundation model has been used to fit the data points only for the single break-through series DOPS1 to DOPS3. The resulting fit has been plotted together with the data points in Figure 37. For the series DOPS4 to DOPS7 a fit has not been attempted because it is difficult to give well defined values for the elastic moduli. The activated volume and the hole formation rate varied from one multivelocity series to another. They are listed together with the other experimental parameters in Table 1.

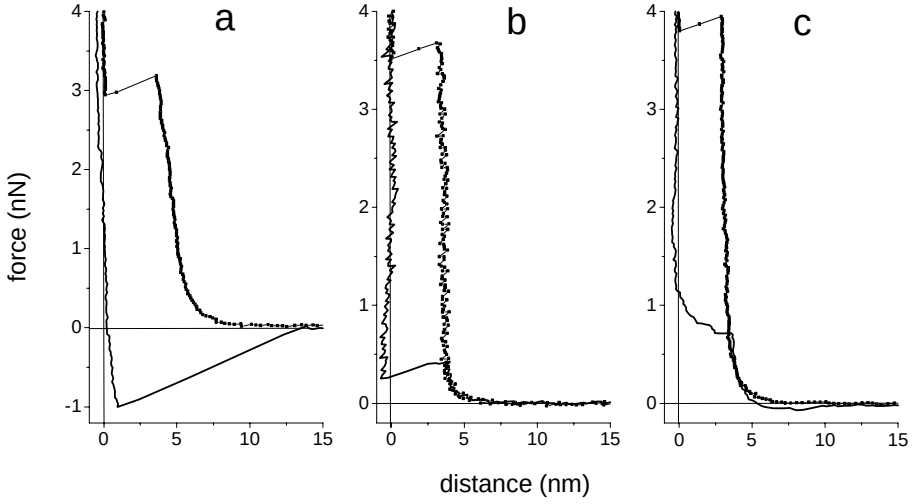

Figure 35. Typical force curves from the multivelocity series that exhibit only one break-through. a) DOPS1, b) DOPS2, c) DOPS3.

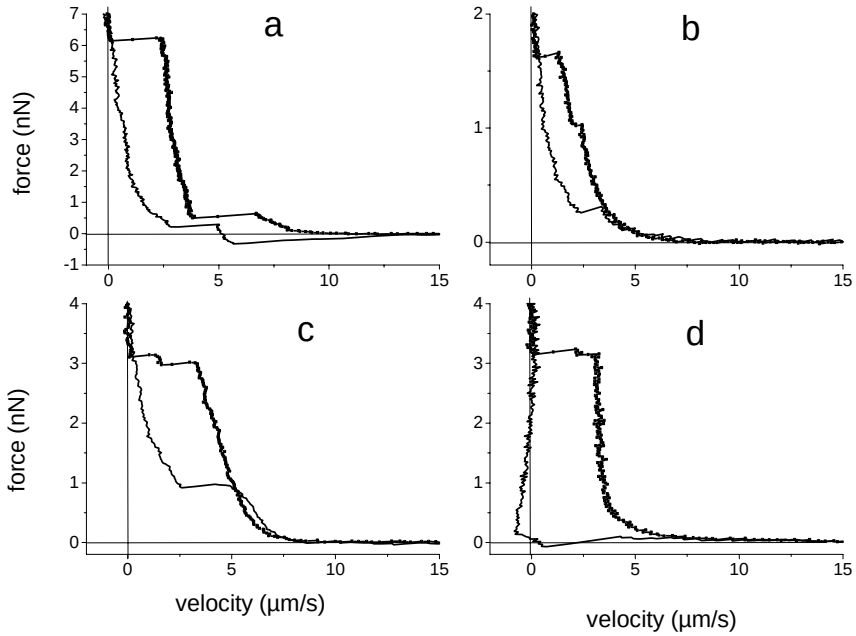

Figure 36. Typical force curves from the multivelocity series that exhibit several break-throughs. a) DOPS4, b) DOPS5, c) DOPS6, c) DOPS7.

The measurements of the first group, DOPS1 to DOPS3, were done with different tips. DOPS1 was carried out with a bare silicon nitride tip. For DOPS2 the tip was functionalized with mercaptoundecanoic acid, and the tip in DOPS3 was functionalized with mercapto-undecanol.

The highest applied forces were about 9 nN but only a part of the force curves is displayed in the figures. The jump heights were in the range between 2.5 nm and 3.5 nm and the bilayer thickness was between 3.5 nm and 5.9 nm. The dependence of the jump height on the velocity is shown in Figure 39. The elastic modulus for DOPS1 was 8 MPa while for DOPS 2 and DOPS3 the moduli were 160 and 180 MPa, respectively.

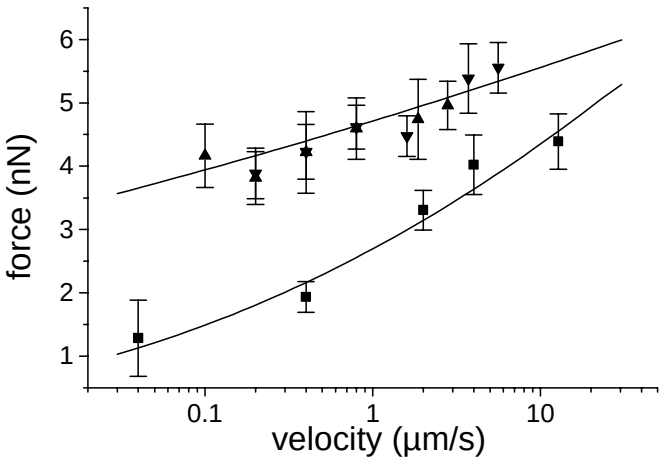

Figure 37. Break-through forces in dependence on the approach velocity. DOPS1 (squares), DOPS2 (up triangles), DOPS3 (down triangles)

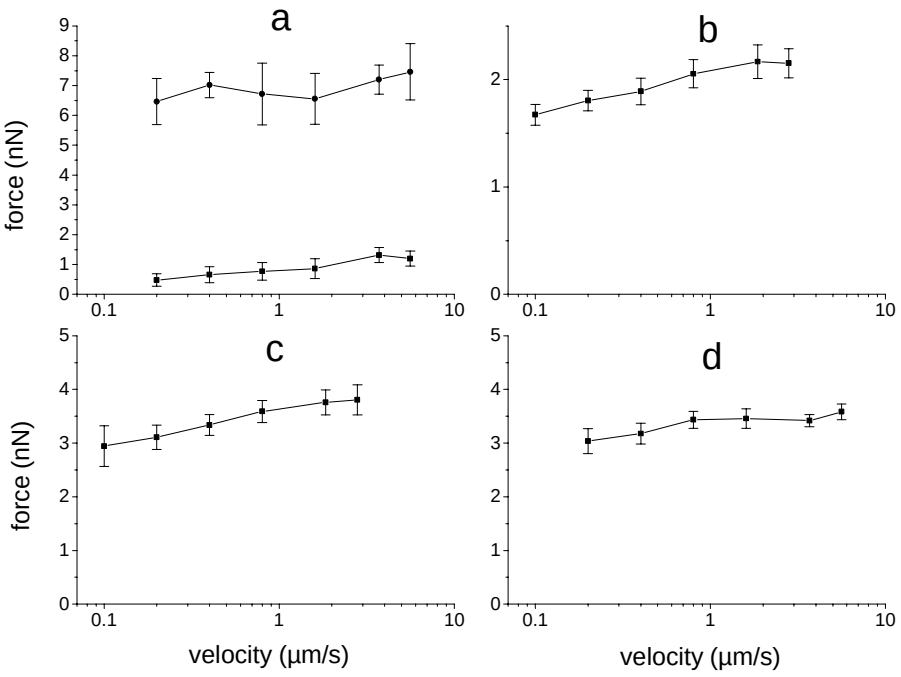

Figure 38. Break-through forces in dependence on the approach velocity for DOPS multivelocity series with more than a single break-through. a) DOPS4, b) DOPS5, c) DOPS6, d) DOPS7

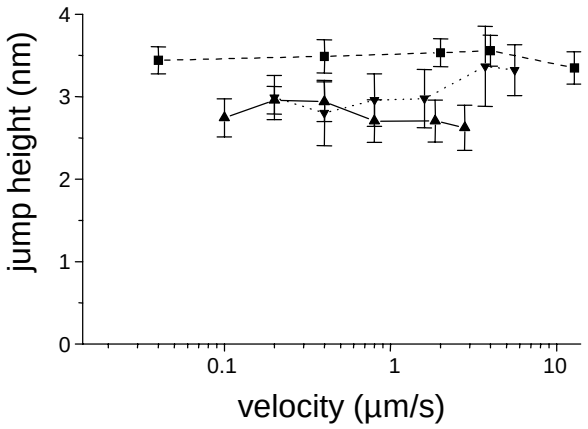

Figure 39. Jump heights for DOPS measurements with a single jump. Dashed line: DOPS1; dotted line: DOPS2; solid line: DOPS3.

The multivelocity series with more features than one single break-through, DOPS4 to DOPS7, have been measured with different tips. DOPS4 and DOPS5 have been measured with uncoated bare silicon nitride tips. The multivelocity series DOPS6 has been recorded with a hydroxy-terminated tip while for DOPS7 a carboxyl-terminated tip has been employed.

The measurements form a group of their own because contrastingly to the prior multivelocity series either two break-throughs or a kink before a break-through were observed. The jump heights of the final break-throughs are plotted versus the approach velocity in Figure 40. The heights varied strongly between the four multivelocity series. In DOPS 4 two distinct break-throughs could be observed. The height of the jump at the lower force was about 3 nm, the height at the higher force was a little bit less than 2 nm. In DOPS5 the average height of the jump-in was only less than 1 nm. Here, the final jump was preceded by a small kink that does not appear in every force curve of the multivelocity series. The force of the final, inner, break-through is quite reproducible while the force at which the kink occurs varies strongly and cannot be evaluated statistically. In the multivelocity series DOPS6 and DOPS7 the tip was briefly stopped during the break-through. This resulted in a kink immediately before the final break-through. The total bilayer thickness for the hydroxyl-functionalized tip in DOPS6 was about 6 nm while for the carboxyl-functionalized tip in DOPS7 it was only about 3.6 nm. According to Figure 40 c) and d) the jump heights scattered in the range between 1 nm and 2.5 nm.

The retract curve for each measurement in the multivelocity series DOPS1 showed a large adhesion while the retract curves for the other multivelocity series exhibited a

jump-out at about 0.5 nN and no adhesion at all. The forces of the jump-out depend on the retract velocity in the way that was predicted in chapter 3 (Figure 41).

Name	Tip	Radius (nm)	Spring Constant of Cantilever	Elastic Modulus of Bilayer (MPa)	bilayerthic k-ness (nm)	αV **(nm^3)**	k_0 **(1/s)**
DOPS1	bare silicon nitride	26	0.09	8	5.9	**4.4**	**0.1**
DOPS2	COOH-terminated thiol	69	0.07	160	3.8	**3.4**	**$1.3\cdot10^{-9}$**
DOPS3	OH-terminated thiol	94	0.07	180	3.5	**3.4**	**$1.3\cdot10^{-9}$**
DOPS4	bare silicon nitride	26	0.07	3*	5.2	-	-
DOPS5	bare silicon nitride	33	0.07	6*	2.8	-	-
DOPS6	OH-terminated thiol	94	0.07	3*	3.0	-	-
DOPS7	COOH-terminated thiol	50**	0.07**	60*	3.7	-	-

* the elastic modulus has been calculated for the force increase up to the first break-through.

** tip radius and spring constant are estimated

Table 2. Parameters for the individual multivelocity series DOPS1 to DOPS7. Only for DOPS1 to DOPS3 a fit with the solid foundation model has been made so that only here the parameters αV and k_0 can be given. For DOPS2 and DOPS3 identical parameters have been used.

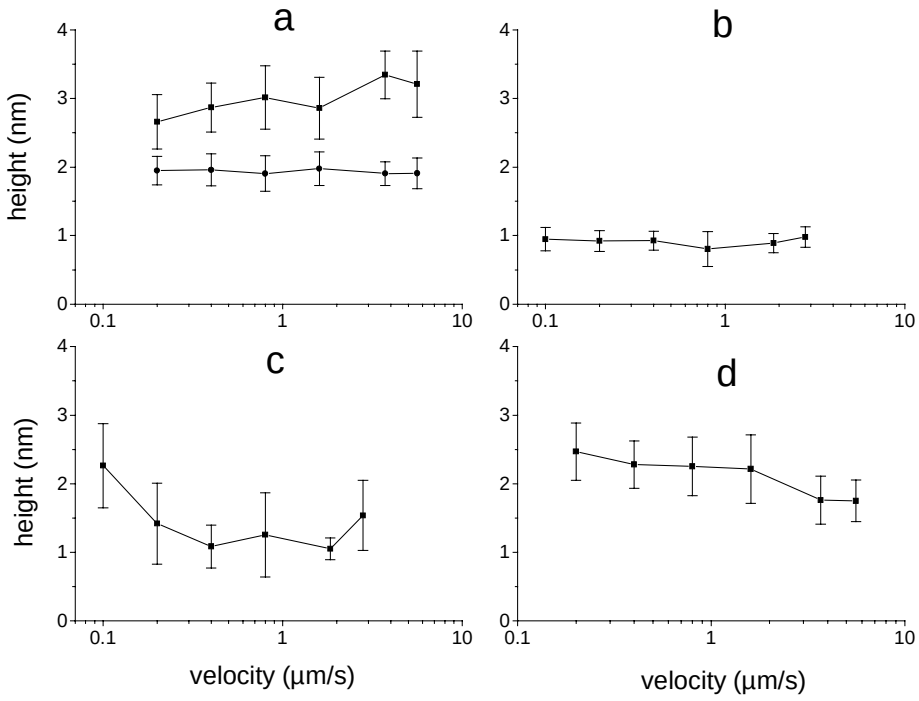

Figure 40. Jump height in dependence of the approach velocity. a) DOPS 4, b) DOPS5, c) DOPS6, d) DOPS7.

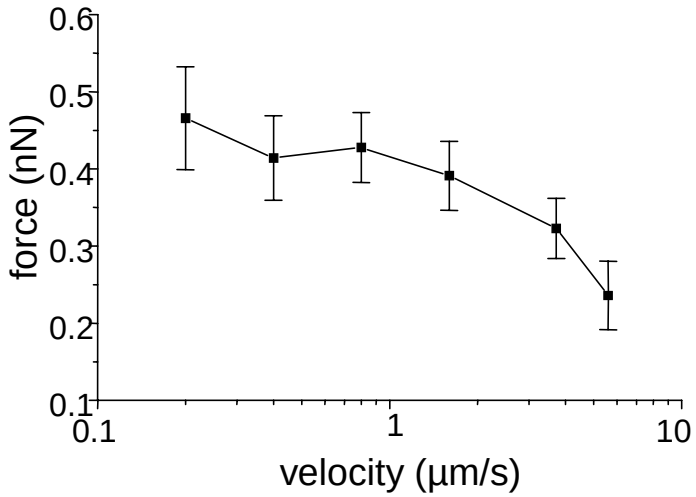

Figure 41. Force of the jump-out in dependence on the velocity for DOPS.

Discussion

Common features of measurements on DOTAP and DOPS. Every force measurement on lipid bilayers consisting of DOTAP and DOPS showed at least one break-through. The force at which a break-through took place always increased with increasing approach velocity. This result agrees with the nucleation model for break-throughs of the AFM tip through lipid bilayers. The solid foundation nucleation model yielded the activated volume and the hopping rate of the tip.

The two lipid species that have been studied in this work differ in their headgroups. Especially, they carry opposite charges. While DOTAP is positively charged and thus it is electrostatically attracted by the negatively charged mica, DOPS carries a negative charge and is therefore repelled by the mica substrate. This difference explains why the values for the hole formation rate are lower for DOTAP than for DOPS.

The activated volume is smaller for DOPS than for DOTAP. Thus, in a bilayer of DOPS smaller holes suffice to initiate a break-through. The reason for this remains unclear without a theoretical description of the break-through.

Apart from common features the measurements for DOTAP and DOPS contain more information that shall be discussed in the following.

Discussion for DOTAP. For DOTAP the force curves have a homogeneous shape. This suggests that the individual bilayers are in a well-defined state that does not differ from one multivelocity series to another. The bilayer thickness is between 4.6 and 5.1 nm. The value for the bilayer thickness may be compared to the total length of a DO-

TAP molecule of about 2.5 nm. This confirms that the measured thickness really corresponds to the thickness of a layer that is two molecules thick, i.e. it corresponds to a bilayer.

The elastic modulus of the bilayer between 20 and 50 MPa is smaller than measured by others (Dufrene, Boland et al. 1998) who made similar measurements on distearoylphosphatidylethanolamine (DSPE) and obtained elastic moduli of about 200 MPa. However, DSPE is in a solid-like state and is therefore expected to be harder than the liquid-like DOTAP. No similar measurements for liquid-like lipids were found in the literature.

By applying forces up to 30 nN on the lipid bilayer a second break-through is revealed. It is difficult to access the exact height of the layer that has been penetrated in this jump but a jump height of 1.9 nm at a force of about 25 nN indicates that a second break-through through a bilayer took place. Thus, presumably two bilayers are formed, one on the tip and another on the mica. They break down separately.

It is questionable which bilayer broke first. If the bilayer on the tip had broken first then it would have been possible to vary the break-through force by a change of the interaction between tip and bilayer which can be achieved by functionalization of the tip. In the multivelocity series DOTAP4 the surface of the tip was covered with mercaptoundecanol. Nevertheless, the force of the first break-through was in the same range as without functionalization. This suggests that the first break-through at lower forces corresponds to the penetration of the bilayer on the mica while at higher forces the bilayer on the tip breaks down. Note that the applied forces were below 15 nN so that the second break-through and possible changes of the break-through was presumably not detectable. The measurements of Dufrêne *et al.* (Dufrene, Boland et al. 1998) also suggest that first the bilayer on mica breaks down. They produced bilayers by the Langmuir-Blodgett technique (LB). There, monolayers are spread on water and then transferred to mica. With this technique multilayers and especially bilayers can be layered in arbitrary order on solid substrates. One of the advantages is that on the AFM tip no bilayer is adsorbed. Additionally, in the measurements of Dufrêne *et al.* the AFM tip is functionalized with hydroxy-terminated thiols so that no adsorption of lipids took place. They measured average break-through forces for the bilayer of 2.6 nN that compares well to the results for the first break-through that are shown in my work.

Figure 31 shows that the dependence of the jump height on the approach velocity is very similar for all three measurements on DOTAP. The jump height tends to decrease with increasing speed. Thus, the deformation increases faster the higher the applied force is. Qualitatively this is reasonable because the force before the break-through is higher at higher velocities. The force leads to a larger elastic deformation of the bilayer. However, none of our models predicts the experimentally observed behaviour. The simplest model, the flat stamp model, predicts that the deformation of the bilayer depends linearly on the applied force since

$$\frac{\delta_0}{h} = \frac{\sigma}{E} = \frac{F}{E \cdot A}. \tag{87}$$

In a first approximation the break-through force depends linearly on the logarithm of the approaching velocity and therefore also the maximum deformation δ_0 should show this dependence, i.e.

$$\frac{\delta_0}{h} \propto \frac{\log v}{E \cdot A} \tag{88}$$

Such a dependence would result in a linear curve in Figure 41 which is not the case.

The result makes clear that the break-through itself is not described by the elastic models that are suited to the deformation of the bilayer. Prior to the break-through possibly structural transformations take place that depend on the applied pressure of the tip. Without a microscopic model of the break-through of an AFM tip through a bilayer exists nothing can be said about this process.

In chapter 3 it has been shown that small variations of the tip radius may lead to considerable differences between the break-through forces. However, the break-through of the bilayer can be caused by a small asperity of the tip surface that is in direct contact with the bilayer. Eventually the radius of this asperity is relevant for the break-through force.

The influence of the chemical composition on the tip is difficult to assess. In order to exclude chemical variations between the experiments and to guarantee a homogeneous composition on the tip surface, the tip in the multivelocity series DOTAP4 was functionalized with mercapto-undecanol. From Figure 30 and Figure 34 it can be seen that the break-through forces in this multivelocity series are very similar to those of DOTAP1 and DOTAP5. On the other hand, the nominal tip radii vary from 23 nm for

DOTAP4 to 60 nm for DOTAP5. Therefore it cannot be concluded whether the coincidence of the break-through forces is accidental or whether the surface chemistry is not relevant for the break-through force.

Discussion for DOPS. On DOPS the force curves regularly exhibit a break-through, too. The force at which the tip breaks through the bilayer is between 1 nN and 5 nN which is similar to the respective values for DOTAP and for other lipids (Dufrene, Boland et al. 1998; Müller, Butt et al. 2000). It may be concluded that lipid molecules are adsorbed on mica but the measurements on DOPS are less homogeneous than those for DOTAP.

Multivelocity series with one or two break-throughs can be observed. The heights of the multivelocity series with one single break-through are in the range between 3.5 and 5.9 nm. The multivelocity series DOPS3 with the large thickness is different from all other multivelocity series on DOPS because the measurements exhibit an adhesion that is as strong as on DOTAP. Those multivelocity series that exhibit two jumps have bilayer thicknesses ranging from 2.8 nm to 6 nm. Assuming a length of a DOPS molecule of about 2.6 nm these values correspond to a monolayer or a bilayer.

Functionalization either with hydroxy-terminated thiols or with carboxyl-terminated thiols seems not to influence the outcome of the experiment.

Outlook

In this work it has been shown that the break-through of an AFM tip through lipid bilayers can be well described by a nucleation model. Still several questions remain open.

For DOPS conditions have to be found that lead to more homogeneous break-throughs. The great variability of the break-throughs suggests the appearance of several phases. The experiments have to be designed in a way that guarantees a constant density of molecules on the surface. Such bilayers can be produced by the transfer of individual monolayers at constant film pressure in a Langmuir trough.

Generally, the state of a bilayer that has been produced by vesicle fusion is a critical parameter. Measurements of the adsorbed mass of natural egg phosphatidylcholine on a silicon oxide substrate indicate that after 20 min a vesicle solution (c=1 µg/ml) is in a well-defined state (Keller, Glasmästar et al. 2000). Our experiments have been started after an adsorption time of 30 min. It is possible that this time is not sufficient to establish a stable bilayer and in future experiments the waiting time should be prolonged.

The geometry and the surface chemistry of the AFM tips must be better controlled. This can be done by gluing small spheres with a defined radius to a cantilever. By variation of the nominal radius of the spherical particle it can be proved whether the break-through force depends on asperities or not. If the break-through force is given by asperities on the sphere then the nominal radius of the sphere will not influence the break-through force.

Possibly, the dependence of the break-through force on well-studied bilayers like egg-phosphatidylcholine can be correlated to diffusion constants and mechanical properties of the lipids.

6. Force on a Tip in *n*-Alcohols over flat Substrates

Motivation

The structure of a liquid at a solid surface is of fundamental scientific interest. Experimentally the liquid structure near surfaces can be analyzed by force measurements. In such a measurement two solid surfaces are brought into close proximity and the force required to approach them from a large distance to a separation d is measured.

For large separations the force between two solid surfaces in a fluid medium can usually be described by continuum theories such as the van der Waals and the electrostatic double-layer theory. At surface separations approaching molecular dimensions continuum theory breaks down and the solvation forces have to be taken into account. Several calculations for apolar molecules, such as hard spheres (Mitchell, Ninham et al. 1977; Snook and Henderson 1978; Henderson and van Swol 1984; Roth 2000), Lennard-Jones fluids (Mitchell, Ninham et al. 1977; Lane and Spurling 1979; van Megen and Snook 1979; van Megen and Snook 1981; Ballamudi and Bitsanis 1996; Dijkstra 1998; Iwamatsu 1998), Gay-Berne (Gruhn 1998), and lattice models (Tarazona and Vicente 1985; Mitlin and Sharma 1995) show that the fluid density profile normal to a solid surface oscillates about the bulk density with a periodicity of about one molecular diameter close to the surface. Far away from the surface it smoothens out to the bulk density. For liquids confined between two surfaces these density variations lead to a periodic force.

Periodic forces at small separations were first experimentally verified with the surface forces apparatus. During recent years solvation forces were also studied with the atomic force microscope. Layered liquid structures were indeed observed for nonpolar liquids with a roughly spherical structure such as octamethylcyclotetrasiloxane and cyclohexane (Horn and Israelachvili 1981; Christenson, Horn et al. 1982; Christenson 1986; O'Shea 1992; Klein and Kumacheva 1998), and toluene (Marra and Hair 1988). Oscil-

lating surface force were also observed in polar liquids such as propylene carbonate (Christenson and Horn 1983) or acetone (Christenson 1984). Even across water a tendency for a periodic force was observed (Pashley and Israelachvili 1984; Grünewald and Helm 1996).

The structure of linear alkanes and alcohols near solid surfaces is of particular interest because of their widespread application. In monodisperse linear alkanes the force oscillates with a periodicity of 4-5 Å which corresponds to the diameter of an alkane chain (Christenson, Gruen et al. 1987). These oscillations dominate the interaction for separations up to 2-3 nm. This suggests that the alkanes have a tendency towards a parallel orientation near the mica surface. In contrast, branched alkanes or mixtures of different alkanes showed almost no layering (Christenson 1983). Molecular dynamics simulations reproduced the results and support the conclusion (Dijkstra 1998).

Long-chain *n*-alcohols (C_nH_{2n+2}, n=8-12) have been systematically investigated with the AFM (O'Shea 1992; Nakada, Miyashita et al. 1996). On graphite a 5 Å thick layer was observed for all alcohols under investigation. Nakada *et al*. could obtain an image of a fishbone ordering of the molecules on graphite. This indicates that the molecules orient parallelly to the graphite surface. On mica these authors observed two phases. At room temperature they observed an oscillatory force with a periodicity of 8.6 Å for all alcohols with nine carbon atoms or more. Increasing the temperature to 40°C leads to a double-layer structure of the long-chain alcohols, that are oriented perpendicular to the mica. These findings are consistent with measurements made with a SFA with 1-octanol and 1-undecanol (Mugele 2000). In an alternative approach Morishige *et al.* have investigated the structure of *n*-alcohols (C_nH_{2n+2}, n=3, 6-9) on graphite by X-ray diffraction (Morishige and Kato 1999). Consistently with the force measurements and the images they find that the molecules arrange in a fishbone pattern on the graphite surface. They were also able to measure the melting behaviour of these two-dimensional smectic-like phases. However, it was impossible to obtain information about the structure of the molecules in layers other than the adsorbed layer directly on the surface. The solvation forces for solutions of methanol, ethanol, and 1-propanol in water have been investigated by Kanda *et al.* (Kanda 1998; Kanda, Iwasaki et al. 1999). They find that short *n*-alcohols tend to form a monolayer of vertically adsorbed molecules on the surface that are replaced by water molecules at increasing water content.

In the present work the previous studies of solvation forces are extended to short chain alcohols for a series from ethanol to 1-octanol (C_nH_{2n+2}, n=2-8). It shall also be verified whether the jumps of the AFM tip in alcohols are thermally activated or not.

Experimental

Alcohols (per analysi grade, for heptanol and octanol for synthesis grade) from Merck, Darmstadt, Germany, were used without further purification. All alcohols were dried over molecular sieves (LAB, 0.3nm, Merck) under dry Argon for at least 24 hours. Mica and highly ordered pyrolytic graphite (HOPG) have been purchased from PLANO, Wetzlar, Germany. They were cleaved immediately before each experiment. Exposure to ambient air was kept as short as possible by covering them with a drop of alcohol immediately after cleavage. The experiments were carried out with the commercial AFM (NanoScope III, Veeco Instr., Santa Barbara, CA), equipped with a fluid cell as described in chapter 5. V-shaped silicon nitride cantilevers (Veeco Instr., CA, length 200 µm or 100 µm, width 40 µm, thickness 0.6 µm) were cleaned in a plasma cleaner in ambient air for 8 min at 30 W. Tips with an average radius of 40 nm were used. All forces are represented as *F/R* in order to use the same notation as in literature. Force curves were recorded as described above. For all force measurements with long cantilevers an approach velocity of 100 nm/s was used, while for the short cantilevers the velocity was 50 nm/s. In order to reduce noise and resolve as many details of force curves as possible approximately 10 force curves were plotted in one graph. To fit the curves with appropriate functions the data array of all force curves was sorted according to the *d*-values of the data points by self-made software (*multipleCurves* programmed in LabWindows, National Instruments, Austin, Texas).

Results and Discussion

Force curves on mica

Force curves measured with all alcohols showed common features (Figure 42 and Figure 43). No significant force was observed for distances larger than roughly 4 nm. At closer distance during the approach of the tip several repulsive maxima and subsequent jumps were observed. The series of two (for octanol) or three (for propanol to heptanol) repulsive maxima is presumably a manifestation of the solvation force caused by the ordering of molecules in the gap between the mica and the tip surface. In the following the last layer of alcohols removed out of the gap is called the ‘inner’ layer. It is

corresponds to the repulsive maximum at the closest distance. For all alcohols at least two outer layers could be identified.

Determination of zero distance is a critical step in AFM force measurements. Presumably after the jump through the inner layer direct contact between the tip and mica surface is established. No further jump is observed for normalized force up to 75 mN/m (~3 nN) and the 'contact' part of the force curve is a straight line showing no indications of deformation.

In chapter 3 the observation of jumps was attributed to two situations: First, jumps occur if the AFM tip penetrates an activation barrier. This is the case for force curves on lipid bilayers where velocity dependent break-through forces are observed. Second, jumps of the tip do also occur without a kinetic barrier when the gradient of an attractive force on the tip exceeds the spring constant of the AFM cantilever. The cantilever jumps until its spring force is balanced by an equally strong repulsive force. The whole region of the attractive force in between cannot be resolved during the approach. However, the attractive force in this regime which is inaccessible during the approach can be probed by retracting the cantilever immediately after the jump has occurred. Experimentally this is realized by a force trigger that is slightly higher than the force at the end point of the jump and lower than the force at which the next jump occurs. This has been carried out for 1-propanol on mica (Figure 43).

Comparison with van der Waals forces

In the experiments the solvation force was much stronger than the van der Waals attraction. To demonstrate this, the van der Waals force was calculated using the theory outlined in chapter 3. For distances below 5 nm retarded van der Waals forces can be neglected. The non-retarded van der Waals force is given by eq. (6) with the non-retarded Hamaker constant A. The Hamaker constant was calculated with eq. (7) using as dielectric constants the expressions from eqs. (8) and (9). For graphite, the plasma frequency ν_p is $1.87 \cdot 10^{16}\ s^{-1}$ (Duley 1998). All other values are taken from chapter 3 and references therein. The resulting Hamaker constants are listed in Table 3. The van der Waals forces are plotted together with the force curves in Figure 42 and Figure 43.

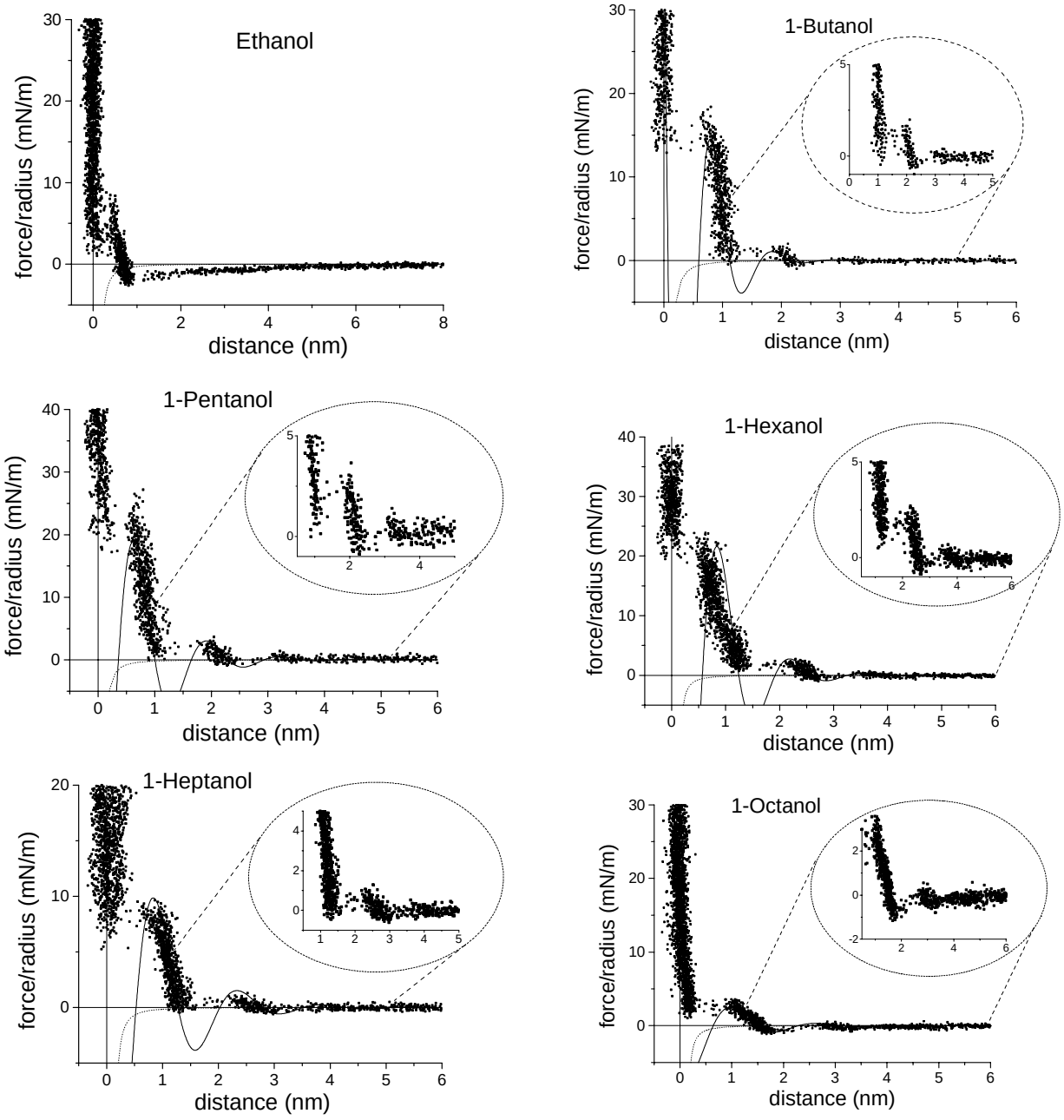

Figure 42. Normalized force-versus-distance curves (force divided by radius of the tip in mN/m) for the interaction of a silicon nitride AFM-tip with mica in 1-ethanol, 1-butanol, 1-pentanol, 1-hexanol, 1-heptanol, and 1-octanol. Each force curve is a superposition of ≈10 individual force curves. All force curves except of ethanol were fitted with the exponentially decaying periodic function from eq. (89) (solid line). The van der Waals attraction is also shown (dotted line).

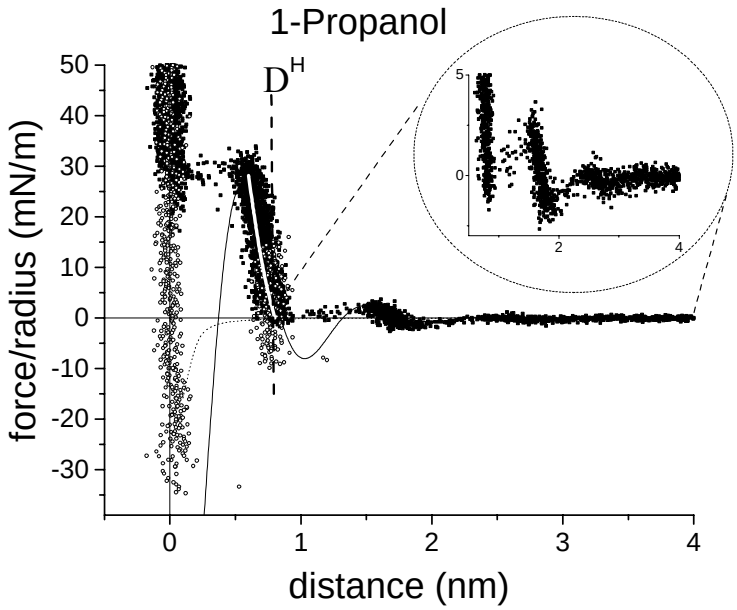

Figure 43. Normalized force-versus-distance curves for the interaction of a silicon nitride AFM-tip with mica in 1-propanol. The force curve is a superposition of ≈10 individual force curves. They were fitted with an exponentially decaying periodic function (continuous line). The force during approach (filled circles) and retract (open circles) was separately measured. The van der Waals attraction is also shown (dotted line). The distance D^H is indicated as a vertical dashed line. The elastic deformation is fitted to the solid foundation model (white solid line).

	ε_3	n_3	A_{mica} / 10^{-21} J	A_{Graphite} / 10^{-19} J
Ethanol	25.3	1.361	3.3	1.19
1-Propanol	20.8	1.385	2.8	1.06
1-Butanol	17.8	1.399	2.5	0.98
1-Pentanol	15.1	1.410	2.3	0.92
1-Hexanol	13.0	1.418	2.1	0.88
1-Heptanol	11.8	1.425	2.0	0.84
1-Octanol	10.3	1.430	1.9	0.82

Table 3. Dielectric permitivities and the refractive indices for the alcohols used at 20°C. Hamaker constants A *were calculated for mica (ε_1=5.4, n_1=1.584 (Bergström 1997)) and graphite interacting with silicon nitride (ε_2=7.4, n_2=1.988) across alcohol.*

Evaluation of the solvation force

To evaluate solvation forces more quantitatively superimposed force curves were fitted with an exponentially decaying periodic function (Israelachvili, 1992, p. 266 and Hartmann, 1993)

$$F = F_0 \cdot \cos\left(\frac{2\pi}{\sigma}[d - \Delta]\right) \cdot e^{-d/\xi} \qquad (89)$$

Here, σ is the oscillation period which at first approximation can be interpreted as the length of density fluctuations in the confined liquid. The decay of density fluctuations is characterized by the decay length ξ. The phase shift Δ in eq. (89) is introduced as an additional fitting parameter. The equation describes a good approximation to the more complex theoretical results.

Results for our measurements are listed in Table 4. The period of the force oscillations increased linearly with increasing chain length of the alcohols (Figure 44). This indicates that the molecules are not oriented parallel to the mica surface but at least partially in an upright position. The period σ is larger than the calculated length of the molecules. I propose two possible arrangements which agree with the observations (Figure 45). The first is a bilayer structure, in which the alcohols are tilted with respect to the surface normal and the hydroxy groups form hydrogen bonds. The tilt angle can also be estimated. Taking the length of the alcohol molecules with *n* carbon atoms to be $L = n \cdot 1.23 + 2.98$ Å the estimated thickness of a bilayer is $2L\cos\Theta$. Here, Θ is the tilt angle with respect to the surface normal. Fitting the measured periodicities with this function leads to an average tilt angle to the substrate normal of 49°. For 1-propanol this interpretation fits well with X-ray studies of the bulk liquid structure (Mikusinska-Planner 1977). These X-ray studies revealed a chain structure in which a row of 1-propanol molecules is connected by hydrogen bonds. The carbon tails of the 1-propanol molecules are tilted with respect to the bond plane so that the height of the whole row can be calculated to be 9 - 10 Å. This agrees with the value of the periodicity for 1-propanol.

The second proposed arrangement is a layered structure in which the alcohol molecules stand upright. They oscillate around their average position so that the particle density is smeared out and the oscillation period of the particle density is larger than the length of a single molecule. The ordering is nematic. The considerable oscillations of the alcohol molecules in the second structure should make hydrogen bonding impossible and the

hydroxy groups of the alcohol molecules do not have to point towards each other. With the present experimental evidence we cannot exclude one structural model.

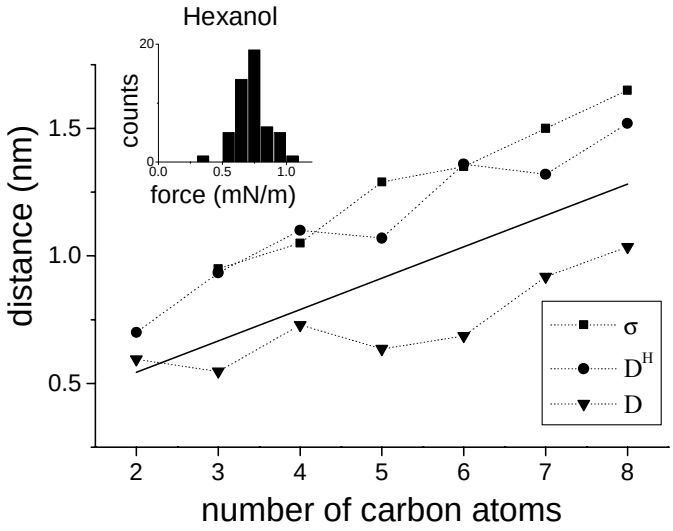

Figure 44. Mean jump-in distance D (down triangles), D^H, the distance of zero force before the inner force maximum (circles), and the periodicity σ (squares) are shown versus the number of carbon atoms. For comparison the straight solid line shows the length of the corresponding, fully extended alcohol. Lines are guides for the eye. The insert shows a typical histogram of jump-in distances D measured with 1-hexanol at an approaching velocity of 200 nm/s.

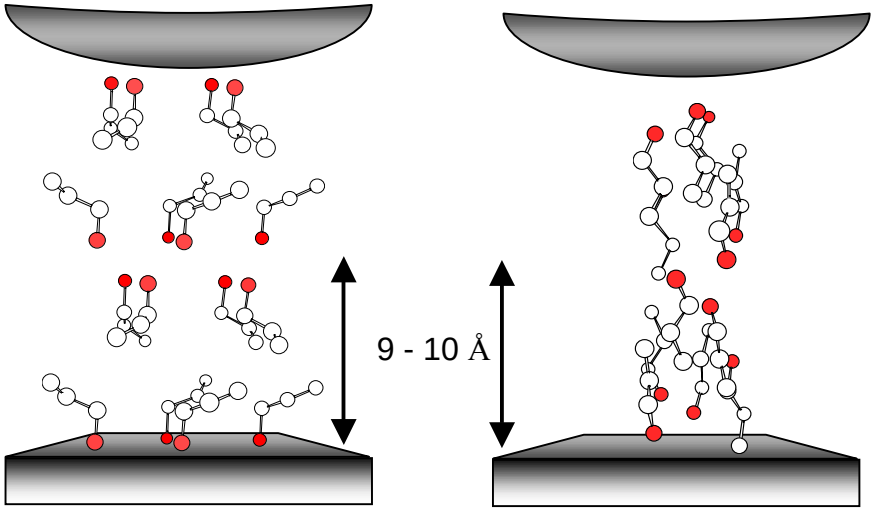

Figure 45. Models for the layering of 1-propanol confined between a spherical tip and mica. The period spacing is 9-10 Å. Hollow circles indicate carbon atoms and black circles oxygen. The hydrogen atoms are left out for clarity. a) The molecules are arranged in the conformation proposed by Mikusinska-Planner(Mikusinska-Planner 1977) b) Layers of alcohols show nematic order and oscillate about their average positions.

Evaluation of the inner layer

Several measures can define the thickness of the inner layer. D is the distance over which the tip jumps through the inner layer. As sketched in Figure 43, D^H is the distance from the bottom of the inner force maximum (F=0 N) to the line of zero distance. At D^H this distance no load is applied to the inner layer and it its deformation is minimal. In Figure 44 the mean values of D and D^H are shown for all alcohols. To get an impression of the scatter of results obtained from individual force curves the insert shows a histogram of jump-in distances D obtained in 1-hexanol.

Break-through forces and jump-in distances D of all alcohols did not significantly depend on the approach velocity of the tip. As an example Figure 46 shows results obtained with *n*-propanol. According to eq. (52) the break-through force is constant if the hole formation rate divided by the activated volume is sufficiently large[1]. This finding suggests that no activation barrier is passed during the penetration through the inner layer.

In general, D and D^H increase with increasing chain length. Since an increasing force compresses the inner layer, the jump distance D is always smaller than the distance D^H. Note that D^H is close to the oscillation period σ of the oscillatory force profile so that the inner layer presumably has the same structure as the outer layers.

To account in a more quantitative way for the deformation of the inner layer the elastic foundation model is used. Fitting the inner repulsive force peak with eq. (18) yields Young's modulus for the alcohols. The indentation δ_0 of the inner layer is calculated from a position where the force applied to the layer is zero. Young's moduli were between 0.01 to 0.1 GPa (Table 4). The alcohol layers show elasticity similar to that of lipid bilayers on mica that in this works was 0.02-0.18 GPa. Reference calculations with the Hertz theory yielded elastic moduli that were by a factor of 4 higher. However, the Hertz theory is only valid for thin layers if the deformation is very small an it cannot be used for the present experiments. Any interpretation using an elastic theory should be taken with care because in elastic theory the molecules cannot escape under load. This cannot be safely assumed for a layer that is not chemisorbed to the surface.

[1] This result has been obtained with the flat stamp nucleation model. However, the results can be extended to the other nucleation models, too.

However, from a purely mechanical point of view alcohols on mica behave similar to adsorbed lipid bilayers.

The amplitude of the force required to break through the inner layer was low for ethanol, increased with increasing chain length until propanol and then decreased again. We have yet no good explanation for the fact that the solvation force is strongest for propanol. However, Gelb *et al.* (Gelb and Lynden-Bell 1994) showed theoretically that the exact tip shape may have a strong impact on the amplitude of the solvation force. Note that they do not find any influence of the tip shape on the oscillation period. Since the precise shape of the tip was not determined in the experiments it might well be that differences between the tip radii might account for the various amplitudes.

	σ / nm	Δ / nm	ξ / nm	E / GPa
Ethanol	-	-	-	0.05
1-Propanol	0.95	0.35	0.39	0.1
1-Butanol	1.05	0.20	0.4	0.1
1-Pentanol	1.29	0.61	0.7	0.1
1-Hexanol	1.35	0.45	0.65	0.05
1-Heptanol	1.50	0.60	0.8	0.03
1-Octanol	1.65	0.60	0.8	0.01

Table 4. Results obtained from fitting superimposed force curves with the exponentially decaying periodic function (4). σ *: Phase shift;* ξ*: Decay length of the exponentially decaying periodic function;* E*: Youngs modulus of the inner layer calculated with eq. (6).*

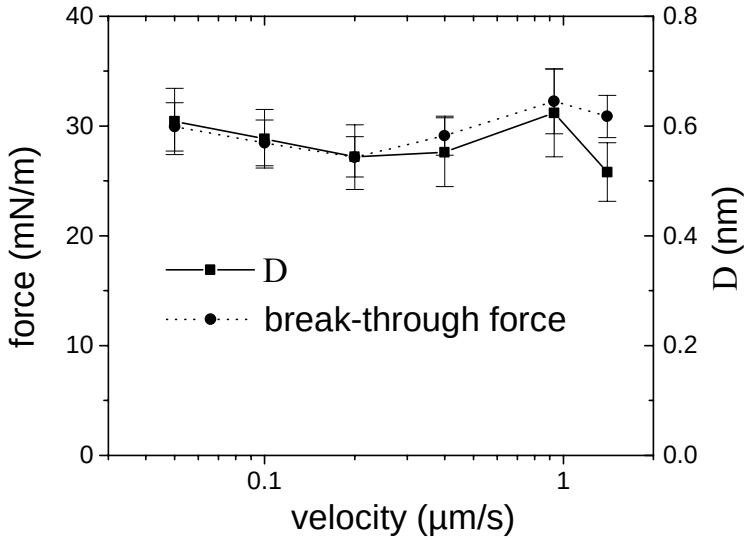

Figure 46. Dependence of the height of the inner jump D *for 1-propanol on mica on the approach velocity of the tip (solid line, right axis). The dotted curve refers to the left axis and shows the break-through force for 1-propanol on mica.*

Temperature dependence

All measurements were made at 22±2 °C. For long-chain alcohols Nakada *et al*. (Nakada, Miyashita et al. 1996) distinguished between a phase at room temperature and at higher temperatures of about 40°C. At the higher temperature the periodicity of the force oscillations depends on the chain length in almost the same way as our measurements at room temperature; the period for the long-chain alcohols from 1-octanol to 1-dodecanol increased by 1.2 Å per carbon atom while here 1.5 Å per carbon atom were measured. Note also that Nakada *et al*. did not observe a flat lying phase for 1-octanol on mica at room temperature. They postulate a transition temperature T_m at which the structure of the alcohol molecules changes from a horizontal to a more upright orientation. This transition temperature depends, like the melting point, on the chain length of the alcohol. Since octanol has a transition temperature below 25°C, T_m for the shorter *n*-alcohols is expected to be even lower so that at room temperature only an upright oriented phase should exist. This was observed so that the results of Nakada *et al.* are in good agreement with the measurements described here. A diagram that summarizes the observations is plotted in Figure 47.

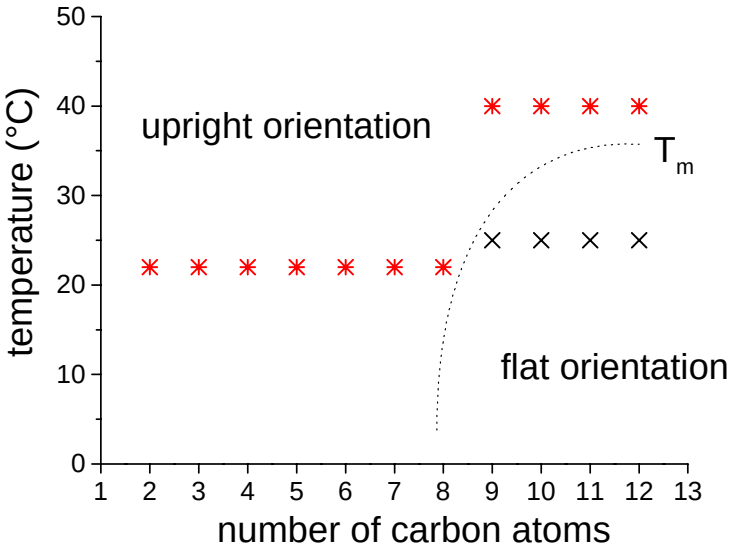

Figure 47. Observed orientation of the n-alcohols in dependence on the temperature. Asterisks denote an upright orientation of the molecules, crosses denote that the molecules arrange flat on the surface. T_m (dotted line) denotes the transition temperature from one orientation to the other.

Peculiar features

Force-curves of three alcohols - ethanol, 1-hexanol and 1-octanol - showed peculiar features. For ethanol a long-range attractive force was observed which was stronger than the calculated van der Waals force. It decays roughly exponentially with a decay length of 2.7 nm. If this repulsion is interpret as an electrostatic force according to the DLVO theory this corresponds to a salt concentration of 0.005 mol/l. It might be due to ions dissociated from mica. Only one jump through an inner layer could be identified. The force at which the jump occurs varied considerably more than for the other alcohols. This indicates a high degree of disorder in the adsorbed ethanol layer.

In the case of 1-hexanol a shoulder before the inner jump was observed. A possible explanation is a rearrangement of the molecules under the pressure of the tip. Similar shoulders have been identified in Monte Carlo simulations of rod-shaped molecules between two walls that interact by a Gay-Berne potential (Gruhn 1998). These authors could show that a nematic phase forms in an isotropic liquid phase that is squeezed out layer by layer when the size of the gap between the walls is decreased. Just before the removal of a layer, however, the molecules in the gap tilt which eventually leads to a shoulder in the force profile.

With 1-octanol only the inner force peak was clearly resolved. The second repulsive force maximum was less reproducible than with the other alcohols. No third repulsive

maximum could be measured. This might indicate that the layering in 1-octanol is less pronounced than in the other alcohols.

It is important to stress that the experimental results were sensitive to the presence of water. Measurements in alcohols that were not dried prior to use showed unreproducible force profiles and often only a single jump could be identified. This issue has been previously addressed by Kanda *et al*. (Kanda 1998) who carried out detailed measurements in water-alcohol mixtures. They could show that the occurrence of jumps is suppressed if the alcohol weight fraction is decreased from 0.99 to 0.3.

Solvation force on graphite

Force curves on graphite have been recorded in the same way as on mica. Here, measurements were made only for 1-propanol and 1-pentanol (Figure 48). During the approach there is no interaction at distances larger than 10 nm. The van der Waals attraction on graphite is significantly stronger than on mica. This attractive force leads to a jump of the cantilever towards the surface at a separation of about 2 nm. However, at a distance of roughly 9 Å the repulsive solvation forces starts to dominate and two subsequent jumps are discernible. For 1-propanol the first jump occurs at a force of about 7 mN/m over a distance of approximately 4 Å. The second, or 'inner', jump occurs at a force of approximately 70 mN/m over a somewhat smaller distance of about 3 Å. Taking the distance between the zero force at the bottom of a repulsive force peak where the deformation of the layer is minimal, both jump distances were 4.5 Å. For 1-pentanol the jumps occur at lower forces but the distances are the same as for 1-propanol.

The forces at which jumps occur differed considerably between subsequent force curves and in many cases only the inner jump was observed. The large variations between the curves make it impossible to superimpose the force curves because instead of enhancing average features the superposition of dissimilar force curves obscurs the details of the individual curves.

We observe a constant period of a multiple of the molecular diameter of about 4.5 Å, independent on the chain length. The measurements indicate that the alcohols are oriented parallel to the surface. These observations confirm the result of others (O'Shea 1992; Nakada, Miyashita et al. 1996; Morishige and Kato 1999).

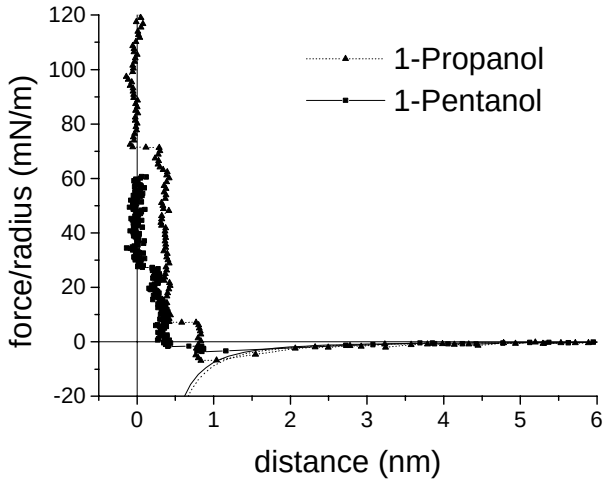

Figure 48. Normalized force-versus-distance curves (force divided by radius of the tip in 10^{-3} N/m) for the interaction of a silicon nitride AFM-tip with HOPG in 1-propanol and 1-pentanol. Each of the curves represents one single measurement. The dotted and the solid line denote the van der Waals force for 1-propanol and 1-pentanol, respectively.

Conclusions.

Solvation forces of linear alcohols ($C_nH_{2n+2}O$, n = 2 - 8) between mica and silicon nitride surfaces show a periodicity of $n \cdot 1.5 + 2.9$ Å, *n* being the number of carbon atoms of the *n*-alcohol. This indicates that the molecules are forming a layered structure in the gap in which they stand at least partially upright. Two different models are proposed. One consists of bilayers of tilted alcohol molecules and the other of a nematic order of the individual molecules. For all alcohols under investigation except of ethanol the double-layer structure extends over at least three periods from the mica substrate into the liquid.

Force curves measured on graphite in 1-propanol and 1-pentanol showed a solvation force with two peaks and a spacing of 4.5 Å. This indicates that on graphite *n*-alcohols show a tendency to align parallel to the surface. This order extends at least over two layers into the liquid.

The force at which the jump takes place did not increase with increasing approach velocity. In the framework of the nucleation models this means that the ratio between hole formation rate and activated volume must be large. Therefore nucleation processes do

not play a role for the jumps. Instead, the jumps can be explained as a mechanical instability.

Outlook

In *n*-alcohols solvation forces are easily detectable. Therefore it is an appropriate system to study the properties of liquid layers more in detail.

Since the layers lead to well reproducible forces the distance between substrate and tip can be well regulated. This allows to measure the viscosity very closely to the substrate that is expected to change in vicinity of a substrate. This can also help to gain deeper insight into the problem of slip in hydrodynamics (Bonaccurso, Kappl et al. 2002).

Measurement of the solvation forces at deeper temperatures would complete the diagram of Figure 47. It could be verified whether all alcohols arrange flat on mica surfaces if the temperature is sufficiently low.

The measurements might initiate a theoretical model for the behaviour of *n*-alcohols in confined geometries.

7. Conclusion

In this work the forces on two different types of liquid layers on smooth substrates have been investigated. The measurements of the surface force were carried out with an atomic force microscope (AFM).

The first type was represented by lipid bilayers on mica. For two lipids force curves on bilayers were measured at different approach velocities between tip and sample. On all bilayers a jump of the tip at a well-defined force was observed. The break-through force increased monotonously with increasing approach velocity.

In order to describe this behaviour a nucleation model is proposed that describes a break-through of the tip through a hole that forms in the bilayer. A kinetic barrier hinders the spontaneous formation of a sufficiently large hole. The model contains two parameters that describe the hole formation rate and an activated volume under the tip that corresponds to the size of a hole through which the tip can jump. The lipid molecule that carries an electric charge opposite to the charge of the substrate has a smaller hole formation rate than the lipid with the same charge. The activated volume is smaller for the lipid with the negatively charged headgroup than for the positively charged one.

The second type of liquid layer was represented by *n*-alcohols. The force measurements reveal an oscillating force as expected for solvation forces. Here the tip jumps towards the substrate, too. However, the force at which the jump takes place is independent of the approach velocity. The nucleation model suggests a negligible activated volume and a high hole formation rate for this case. Instead, the jumps are due to a force gradient that exceeds the restoring force of the cantilever to which the tip is attached. The oscillatory force profile suggests that in confined geometries the molecules assume a structural order. Comparison of *n*-alcohols with different chain lengths yields that on graphite the molecules arrange horizontally while on mica they stand more vertically.

The kinetic theory that has been developed in this work gives a new interpretation for the ubiquitous jumps in AFM force measurements that help to understand thin liquid films in contact with a substrate better.

8. Literature

Parts of this work were published.

- Franz, V., S. Loi, H. Müller, E. Bamberg, H.-J. Butt (2002). "Tip Penetration through Lipid Bilayers in Atomic Force Microscopy." Col. Surf. B: Biointerfaces **23** (2002) 191-200
- Franz, V., H.-J. Butt (2002) "Confined liquids: Solvation forces in liquid alcohols between solid surfaces." accepted for publication in J. Phys. Chem.

Ballamudi, R. K. and I. A. Bitsanis (1996). "Energetically driven liquid-solid transitions in molecularly thin n-octane films." J. Chem. Phys. **105**: 7774-7782.

Bergström, L. (1997). "Hamaker constants of inorganic materials." Adv. Colloid Interface Sci. **70**: 125-169.

Binnig, G., C. F. Quate, et al. (1986). "Atomic Force Microscope." Phys. Rev. Lett. **56**(9): 930-933.

Binnig, G., H. Rohrer, et al. (1982). "Surface Studies by Scanning Tunneling Microscopy." Phys. Rev. Lett. **49**: 57-61.

Bonaccurso, E., M. Kappl, et al. (2002). "Hydrodynamic force measurements: Boundary slip of water on hydrophilic surfaces and electrokinetic effects." Phys. Rev. Lett. accepted for publication.

Brian, A. A. and H. M. McConnell (1984). "Allogeneic stimulation of cytotoxic T cells by supported planar membranes." Proc. Natl. Acad. Sci. USA **81**: 6159-6163.

Butt, H. J., Jaschke, M. (1995). "Calculation of thermal noise in atomic force microscopy." Nanotechnology **6**: 1-7.

Butt, H. J., A. Döppenschmidt, et al. (2000). "Analysis of plastic deformation in atomic force microscopy: Application to ice." J. Chem. Phys. **113**(3): 1194-1203.

Butt, H. J. and V. Franz (2001). Atomic Force Microscope Analysis of Water-Mediated Interfacial Interactions. Water in Biomaterials Surface Science. M. Morra. Chichester, New York, Weinheim, John Wiley & Sons, Ltd.**:** 245-266.

Cappella, B. and G. Dietler (1999). "Force-distance curves by atomic force microscopy." Surface Science Reports **34**: 1-104.

Christenson, H. K. (1983). "Experimental measurements of solvation forces in nonpolar liquids." J. Chem. Phys. **78**: 6906-6913.

Christenson, H. K. (1984). "DLVO theory and solvation forces between mica surfaces in polar and hydrogen-bonding liquids." J. Chem. Soc., Faraday Trans I **80**: 1933-1946.

Christenson, H. K. (1986). "Interactions between hydrocarbon surfaces in a nonpolar liquid: Effect of surface properties on solvation forces." J. Phys. Chem. **90**: 4-6.

Christenson, H. K., D. W. R. Gruen, et al. (1987). "Structuring in liquid alkanes between solid surfaces: Force measurements and mean-field theory." J. Chem. Phys. **87**: 1834-1841.

Christenson, H. K. and R. G. Horn (1983). "Direct measurement of the force between solid surfaces in a polar liquid." Chem. Phys. Lett. **98**: 45-48.

Christenson, H. K., R. G. Horn, et al. (1982). "Measurement of forces due to structure in hydrocarbon liquids." J. Colloid Interface Sci. **88**: 79-88.

Claesson, P. M., T. Ederth, et al. (1996). "Techniques for measuring surface forces." Adv. Colloid Interface Sci. **67**: 119-183.

Derjaguin, B. V., V. M. Muller, et al. (1975). "Effect of contact deformations on the adhesion of particles." J. Colloid Interface Sci. **53**: 314-325.

Dijkstra, M. (1998). "Structure and solvation forces in confined films of alkanes." Thin Solid Films **330**: 14-20.

Dufrene, Y. F., T. Boland, et al. (1998). "Characterization of the physical properties of model biomembranes at the nanometer scale with the atomic force microscope." Faraday Discuss. **111**: 69-78.

Duley, W. W., Seahra, S. (1998). "Graphite, Polycyclic Aromatic Hydrocarbons and the 2175A Extinction Feature." Astrophys. J. **507**: 874-888.

Florin, E. L., V. T. Moy, et al. (1994). “Adhesion Forces Between Individual Ligand-Receptor Pairs.” Science **264**: 415-417.

Gady, B., D. Schleef, et al. (1998). “The Interaction between Micrometer-size Particles and Flat Substrates: A Quantitative Study of Jump-to-Contact.” J. Adhesion **67**: 291-305.

Galla, H. J., W. Hartmann, et al. (1979). “On Two-Dimensional Passive Random Walk in Lipid Bilayers and Fluid Pathways in Biomembranes.” J. Membrane Biol. **48**: 215-236.

Gelb, L. D. and R. M. Lynden-Bell (1994). “Effects of atomic-force-microscope tip characteristics on measurement of solvation-force oscillations.” Phys. Rev. B **49**(3): 2058-2066.

Grier, D. G. (1997). “Optical tweezers in colloid and interface science.” Curr. Opin. Coll. Interf. Sci. **2**(3): 264-270.

Grimson, M. J. and P. Richmond (1980). “Solvation Forces in Molecular Fluids.” J. Chem. Soc. Faraday II **76**: 1478-1484.

Grimson, M. J., G. Rickayzen, et al. (1980). “Short range solvation forces in fluids. I. General formalism and hard particle fluids.” Mol. Phys. **39**(1): 61-73.

Gruhn, T., Schoen, M. (1998). “Substrate-induced order in confined nematic liquid-crystal films.” J. Chem. Phys. **108**(21): 9124-9136.

Grünewald, T. and C. A. Helm (1996). “Computer-controlled experiments in the surface force apparatus with a CCD-spectrograph.” Langmuir **12**: 3885-3890.

Henderson, J. R. and F. van Swol (1984). “On the interface between a fluid and a planar wall. Theory and simulations of a hard sphere fluid at a hard wall.” Mol. Phys. **51**: 991-1010.

Horn, R. G. and J. N. Israelachvili (1981). “Direct measurement of structural forces between two surfaces in a nonpolar liquid.” J. Chem. Phys. **75**: 1400-1411.

Hui, S. W., Viswanathan, J.A., Zasadzinski, J.A., Israelachvili, J.N. (1995). “The structure and stability of phospholipid bilayers by atomic force microscopy.” Biophys. J. **68**: 171-178.

Israelachvili, J. N. (1992). Intermolecular and Surface Forces. London, Academic Press.

Israelachvili, J. N. and D. Tabor (1972). “The measurement of van der Waals dispersion forces in the range of 1.5 to 130 nm.” Proc. Roy. Soc. London A **331**: 19-38.

Iwamatsu, M. (1998). “A molecular theory of solvation force oscillations in nonpolar liquids.” J. Colloid Interface Sci. **204**: 374-388.

Jaschke, M., Butt, H.-J. (1995). “Height calibration of optical lever atomic force microscopes by simple laser interferometry.” Rev. Sci. Instrum. **66**: 1258-1259.

Johnson, K. L. (1985). Contact Mechanics. Cambridge, New York, Melbourne, Cambridge University Press.

Johnson, K. L. and J. A. Greenwood (1997). “An Adhesion Map for the Contact of Elastic Spheres.” J. Colloid Interface Sci. **192**(2).

Johnson, K. L., K. Kendall, et al. (1971). “Surface energy and contact of elastic solids.” Proc. Royal Soc. London A **324**: 301-313.

Kanda, Y., Nakamura, T., Higashitani, K. (1998). “AFM studies of interaction forces between surfaces in alcohol-water solutions.” Coll. Surf. A **139**: 55-62.

Kanda, Y., S. Iwasaki, et al. (1999). “Adhesive force between hydrophilic surfaces in alcohol-water solutions.” J. Colloid Interface Sci. **216**: 394-400.

Keller, C. A., K. Glasmästar, et al. (2000). “Formation of Supported Lipid Membranes.” Phy. Rev. Lett. **84**(23): 5443-5446.

Klein, J. and E. Kumacheva (1998). “Simple liquids confined to molecular thin layers. I. Confinement-induced liquid-to-solid phase transitions.” J. Chem. Phys. **108**: 6996-7009.

Lane, J. E. and T. H. Spurling (1979). “Forces between adsorbing walls: Monte Carlo calculations.” Chem. Phys. Lett. **67**: 107-108.

Marra, J. and M. L. Hair (1988). “Interactions between adsorbed polystyrene layers in toluene-heptane mixtures. Effect of solvent quality.” Macromolecules **21**: 2349-2355.

Mikusinska-Planner, A. (1977). “X-ray Diffraction Study of the Structure of 1-Propanol at -25°C.” Acta Cryst. **A33**: 433-437.

Mitchell, D. J., B. W. Ninham, et al. (1977). “Hard sphere structral effects in colloid systems.” Chem. Phys. Lett. **51**: 257-260.

Mitlin, V. S. and M. M. Sharma (1995). “Lattice-fluid model for solvation force oscillations in nonionic fluid films.” J. Colloid Interface Sci. **170**: 407-420.

Morishige, K. and T. Kato (1999). “Chain-length dependence of melting of *n*-alcohol monolayers adsorbed on graphite: *n*-hexanol, *n*-heptanol, *n*-octanol, and *n*-nonanol.” J. Chem. Phys. **111**: 7095-7099.

Mugele, F., Salmeron, M. (2000). “Dynamics of Layering Transitions in Confined Liquids.” Phys. Rev. Lett. **84**(25): 5796-5799.

Müller, H., H. J. Butt, et al. (2000). “Adsorption of Membrane-Associated Proteins to Lipid Bilayers Studied with an Atomic Force Microscope: Myelin Basic Protein and Cytochrome c.” J. Phys. Chem. B **104**(18): 4552-4559.

Muresan, A. S. and K. Y. C. Lee (2001). “Shape Evolution of Lipid Bilayer Patches Adsorbed on Mica: an Atomic Force Microscopy Study.” J. Phys. Chem. B **105**: 852-855.

Nakada, T., S. Miyashita, et al. (1996). “Atomic Force Microscopic Study of Subsurface Ordering and Structural Transforms in n-Alcohol on Mica and Graphite.” Jpn. J. Appl. Phys. **35**: L52-L55.

O'Shea, S. J., Welland, M.E., Rayment, T. (1992). “Solvation forces near a graphite surface measured with an atomic force microscope.” Appl. Phys. Lett. **60**(19): 2356-2358.

Pashley, R. M. and J. N. Israelachvili (1984). “Molecular layering of water in thin films between mica surfaces and its relation to hydration forces.” J. Colloid Interface Sci. **101**: 511-523.

Persson, B. N. J. and E. Tosatti (1994). “Layering transition in confined molecular thin films: Nucleation and growth.” Phys. Rev. B **50**(8): 5590-5599.

Porcheron, F., Rousseau, B., Schoen, M., Fuchs, A.H. (2001). “Structure and solvation forces in confined alkane films.” PCCP **3**(7): 1155-1159.

Rädler, J., M. Radmacher, et al. (1994). “Velocity-Dependent Forces in Atomic Force Microscopy Imaging of Lipid Films.” Langmuir **10**(9): 3111-3115.

Roth, R., Dietrich, S. (2000). “Binary hard-sphere fluids near a hard wall.” Phys. Rev. E **62**(5): 6926-6936.

Sader, J. E., J. W. M. Chon, et al. (1999). “Calibration of rectangular atomic force microscope cantilevers.” Rev. Sci. Instrum. **70**(10): 3967-3969.

Schneider, J., Y. F. Dufrene, et al. (2000). “Atomic Force Microscope Image Contrast Mechanisms on Supported Lipid Bilayers.” Biophys. J. **79**(2): 1107-1118.

Schoen, M., Gruhn, T., Diestler, D. (1998). “Solvation forces in thin films confined between macroscopically curved substrates.” J. Chem. Phys. **109**(1): 301-311.

Snook, I. K. and D. Henderson (1978). “Monte Carlo study of hard-sphere fluid near a hard wall.” J. Chem. Phys. **68**: 2134-2139.

Tabor, D. and R. H. S. Winterton (1968). “Surface forces: Direct measurement of normal and retarded van der Waals forces.” Nature **219**: 1120-1121.

Tarazona, P. and L. Vicente (1985). “A model for density oscillations in liquids between solid walls.” Mol. Phys. **56**(3): 557-572.

Torii, A., M. Sasaki, et al. (1996). “A method for determining the spring constant of cantilevers for atomic force microscopy.” Meas. Sci. Technol. **7**: 179-184.

van Megen, W. and I. Snook (1979). “Solvent Structure and Solvation Forces between Solid Bodies.” J. Chem. Chem. Soc. Faraday Trans. 2 **75**: 1095-1102.

van Megen, W. J. and I. K. Snook (1981). “Solvation force in simple dense fluids. II. Effect of chemical potential.” J. Chem. Phys. **74**: 1409-1411.

Viitala, T. and J. Peltonen (1999). “UV-induced reaction kinetics of dilinoleoylphosphatidyl ethanolamine monolayers.” Biophys. J. **76**: 2803-2813.

Wedler, G. (1997). Lehrbuch der physikalischen Chemie. Weinheim, Wiley-VCH.

Weisenhorn, A. L., M. Egger, et al. (1991). “Molecular-resolution images of Langmuir-Blodgett films and DNA by atomic force microscopy.” Langmuir **7**: 8-12.

Zasadzinski, J. A. N., C. A. Helm, et al. (1991). “Atomic force microscopy of hydrated phosphatidylethanolamine bilayers.” Biophys. J. **59**: 755-760.

Danksagung

Mein größter Dank gilt dem Betreuer dieser Doktorarbeit, Prof. Dr. Hans Jürgen Butt. Als ich noch an anderem Ort über Probleme der Grenzflächenphysik forschte, konnte ich bereits über experimentelle Fragen mit ihm diskutieren. Schließlich gab er mir die Gelegenheit, am Institut für Physikalische Chemie in Mainz und dann in Siegen unter seiner Betreuung arbeiten zu können. Die außerordentliche Offenheit und die fruchtbare, kollegiale Atmosphäre, die in den Arbeitsgruppen unter seiner Leitung immer herrschte, hatte maßgeblichen Anteil am Gelingen dieser Arbeit und vor allem auch daran, daß ich dabei immer viel Freude hatte.

Prof. Dr. Ernst Bamberg und dem Max-Planck Institut für Biophysik in Frankfurt danke ich dafür, daß ich einen Teil der Messungen an seinem Institut anfertigen durfte.

Dr. Roberto Raiteri danke ich für die anfängliche Betreuung der Arbeit und Hilfestellung bei Computerproblemen. Dafür, daß Computerprobleme in Siegen so selten auftraten und für manche schönen Gespräche danke ich Dr. Michael Kappl. Dr. Karl-Heinz Graf danke ich für die viele Zeit, die er mit Diskussionen mit mir zugebracht hat. Beiden danke ich dafür, ihr großes Wissen jederzeit weiterzugeben.

Dr. Elmar Bonaccurso und Dr. Henning Müller danke ich für ihre Kollegialität und dafür, daß sie mir einige Abbildungen für diese Arbeit zur Verfügung stellten. Jalal Arjomandi, Hanne Christian, Iona Covalcica, Astrid Döppenschmidt, Stefan Ecke, Dr. Christian Mähner, Brigitte Niesenhaus, Dr. Markus Preuss, Peter Rickert, Gexiao Sun, Olga Vinogradova und Gleb Yakubov danke ich für die Zeit in Mainz und Siegen.

Ich danke den benachbarten Instituten in Mainz und Siegen für die gute Atmosphäre, viele Gespräche und die Möglichkeit, benötigte Geräte unkompliziert ausleihen oder benutzen zu können. Für letzteres danke ich besonders Felix Koberling und Dr. Christof Reiner.

Für manche praktische Hilfestellung am Max-Planck Institut in Frankfurt danke ich in Vertretung für alle dort besonders Dr. Klaus Fendler, Eva Grabsch und Dirk Zuber.

Dafür, daß ich mich in Siegen weniger mit bürokratischen Problemen herumschlagen mußte, danke ich Annelie Schäfer.

Dr. Simona Loi danke ich ganz besonders, für alles.

Allen Freunden in Aachen, Jülich, Würzburg, Mainz und Siegen, danke ich, daß ich mit ihnen eine schöne Zeit verbringen konnte.

Meinen Eltern danke ich für jede Art von Unterstützung, die meine Ausbildung möglich gemacht hat.